Hitomi High Energy Resolution X-ray Spectroscopy of the Perseus core

Takayuki TAMURA

All results by the Hitomi collaboration

1. Motivations: X-ray spectroscopy and cluster dynamics
2. *Hitomi*, and 1st X-ray carorimeter. Observations of the Perseus
3. Results (1) Line profile and the ICM velocities
4. Results (2) Spectral fitting with collisional ionization equilibrium models and thermal structure
5. Discussion & Summary

1. Motivations

Cluster Dynamics

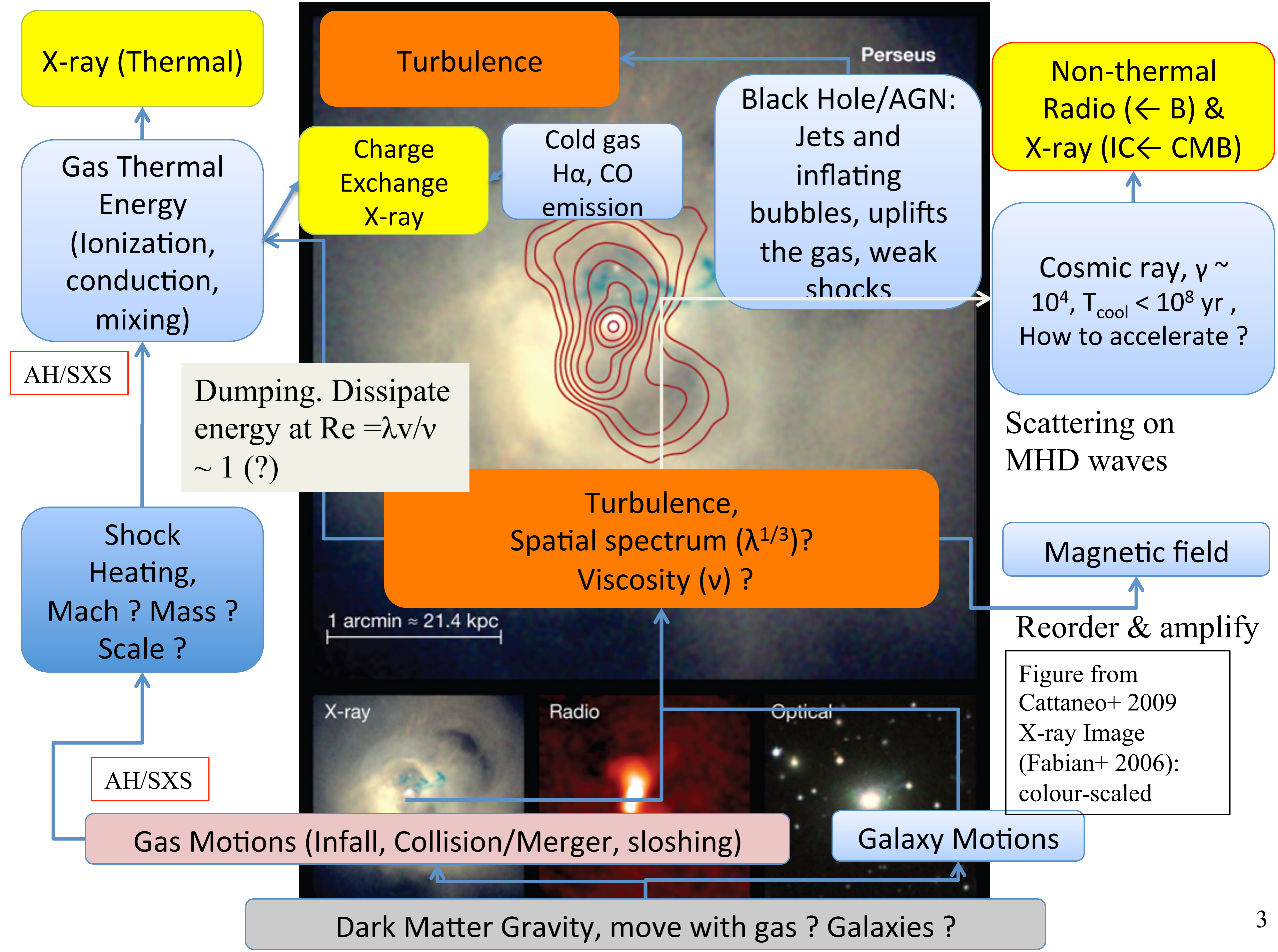
X-ray (Thermal)
Turbulence
Perseus
Non-thermal Radio (← B) & X-ray (IC← CMB)
Charge Exchange X-ray
Cold gas Hα, CO emission
Black Hole/AGN: Jets and inflating bubbles, uplifts the gas, weak shocks
Gas Thermal Energy (Ionization, conduction, mixing)
Cosmic ray, γ ~ 10^4, T_cool < 10^8 yr , How to accelerate ?
AH/SXS
Dumping. Dissipate energy at Re =λv/ν ~ 1 (?)
Scattering on MHD waves
Turbulence, Spatial spectrum (λ^1/3)? Viscosity (ν) ?
Magnetic field
Shock Heating, Mach ? Mass ? Scale ?
1 arcmin ≈ 21.4 kpc
Reorder & amplify
Figure from Cattaneo+ 2009 X-ray Image (Fabian+ 2006): colour-scaled
X-ray
Radio
Optical
AH/SXS
Gas Motions (Infall, Collision/Merger, sloshing)
Galaxy Motions
Dark Matter Gravity, move with gas ? Galaxies ?

Predictions: Detect and locate ICM turbulence

$$
\begin{aligned}
W_{\rm inst} &\simeq 5\ {\rm eV}, \\
W_{\rm therm} &= \sqrt{8\ln 2}\left(\frac{kT_{\rm ion}}{m_{\rm ion}c^2}\right)^{1/2} E_{\rm obs}, \\
&= 4.9\ {\rm eV}\left(\frac{kT_{\rm ion}}{5\ {\rm keV}}\right)^{1/2}\left(\frac{m_{\rm ion}}{56\ m_{\rm p}}\right)^{-1/2}\left(\frac{E_{\rm obs}}{6.7{\rm keV}}\right), \\
W_{\rm turb} &= \sqrt{8\ln 2}\left(\frac{v_{\rm turb}}{c}\right) E_{\rm obs}, \\
&= 5.3\ {\rm eV}\left(\frac{v_{\rm turb}}{100\ {\rm km/s}}\right)\left(\frac{E_{\rm obs}}{6.7\ {\rm keV}}\right),
\end{aligned}
$$

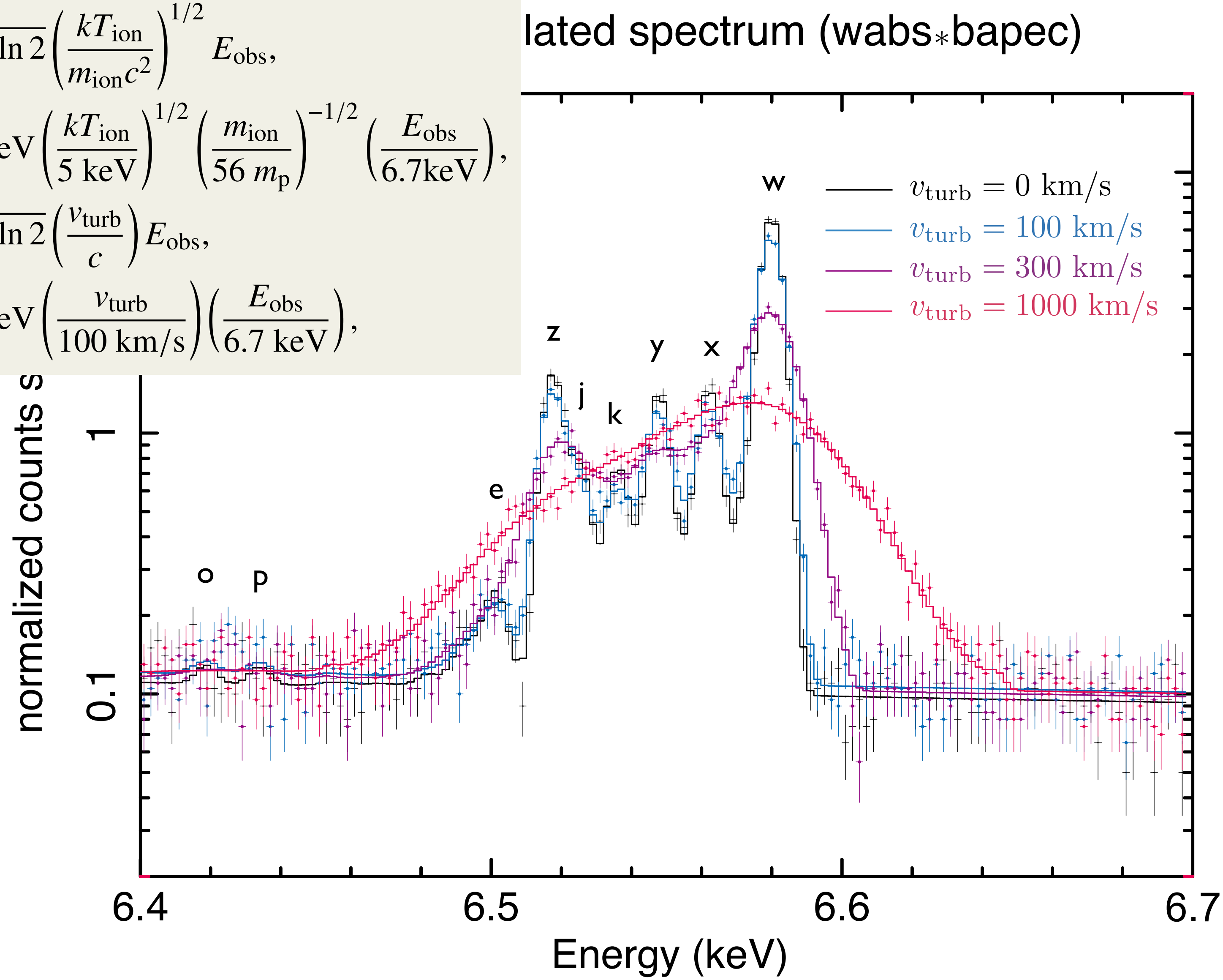

2 *Hitomi* (瞳): An X-ray observatory

ASTRO-H ⇨ Hitomi	The 6th Japanese X-ray astronomy satellite by a international collaboration
Launch	2016-02-17 @ Tanegashima Space Center, Japan By JAXA H-IIA rocket
Orbit	Attitude 576.5-574.4 km, approximately circular, 31 deg. inclination
Total Length	14 m
Mass	2.7 ton
Power	< 3500 W

(Takahashi+ 2016)

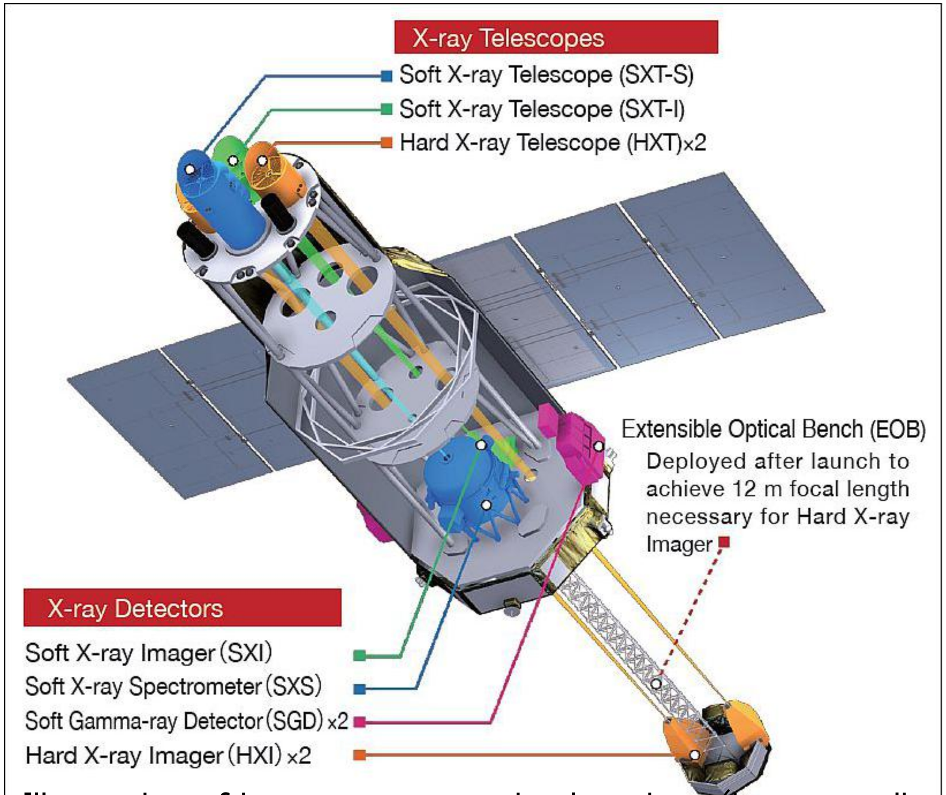

Illustration of instrument mounting locations (image credit: JAXA/ISAS)

After successfully executing start-up operations, the satellite lost contact with the ground with signatures of partial break up of the spacecraft. On April 28, JAXA decided to discontinue the recovery operation.

Soft X-ray Spectrometer (SXS; an X-ray micro calorimeter Kelly + 2016)

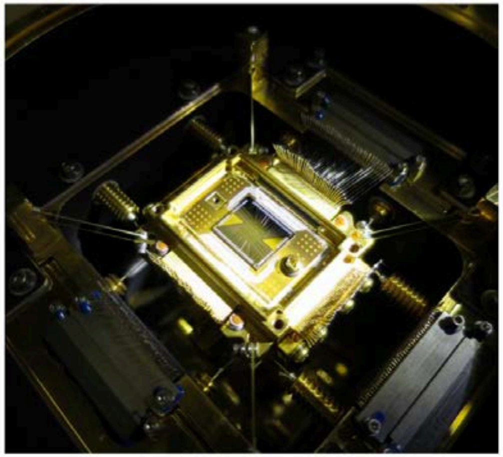

Figure 5. Photographs of (left) SXS sensor and (right) SXS Dewar. The sensor was suspended from the outer st using Kevlar, and electrical connections to the housing were made using tensioned wires to reduce the sensit microphonics.The outer shell of the Dewar is 950 mm in diameter.

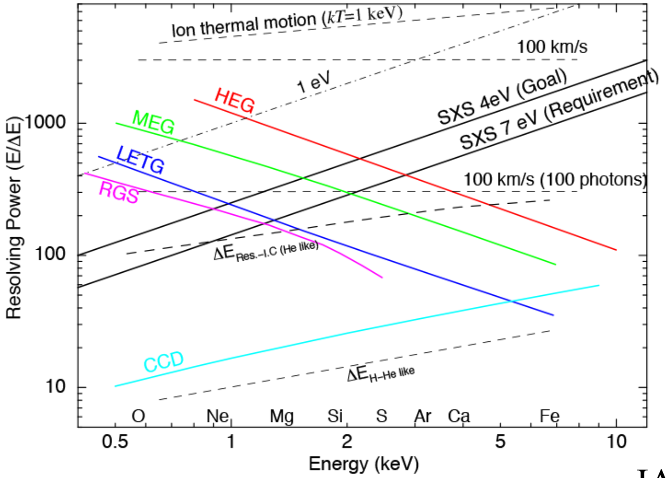

Takahashi+ 2016

JAXA documents(2016)

Figure 3: Resolving power of the SXS as a function of X-ray energy for the two cases, 4 eV resolution (goal or extra success) and 7 eV (nominal requirement).

Operating temperature	50 mK
Energy resolution	4.9 eV (FWHM), E/dE=1250 @ 6keV
Energy band	0.3-12 keV (2-12 keV; before valve/window open for all observations)
Angular performance	6x6 pixels (3’ x 3’) 1’.2 Half power diameter
Energy scale calibration	Calibration source to all pixels. (One calibration pixel)

Observations of the Perseus cluster core

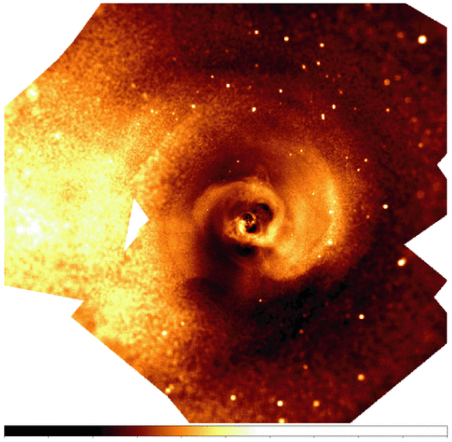

Chandra radial fraction difference (Fabian+ 2011). The image is 25.6 arcmin from north to south.

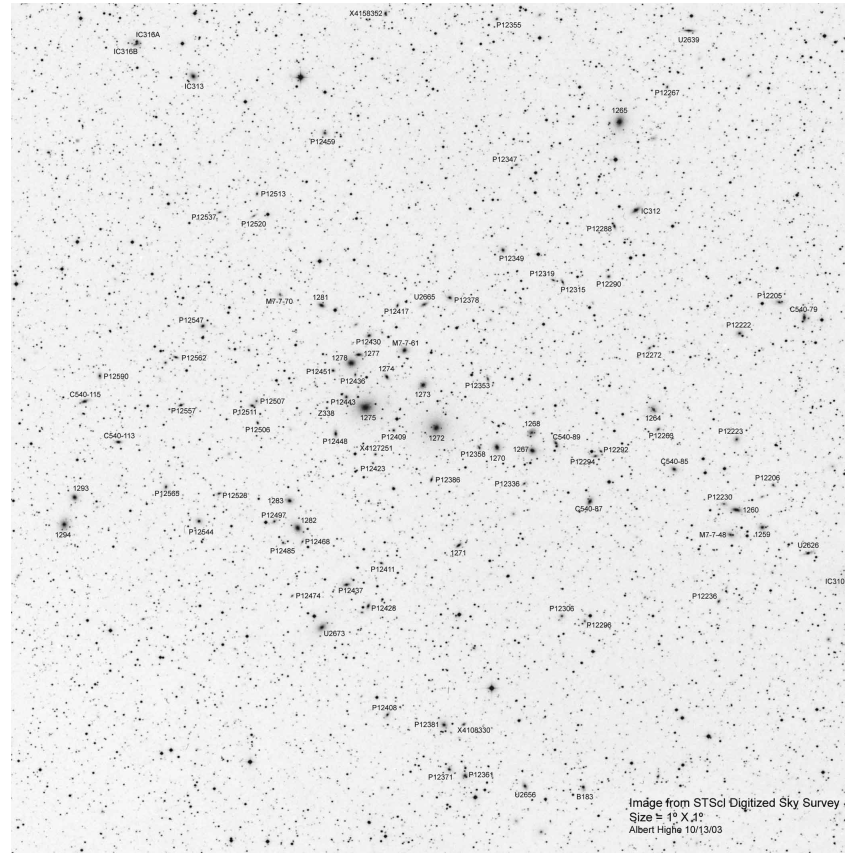

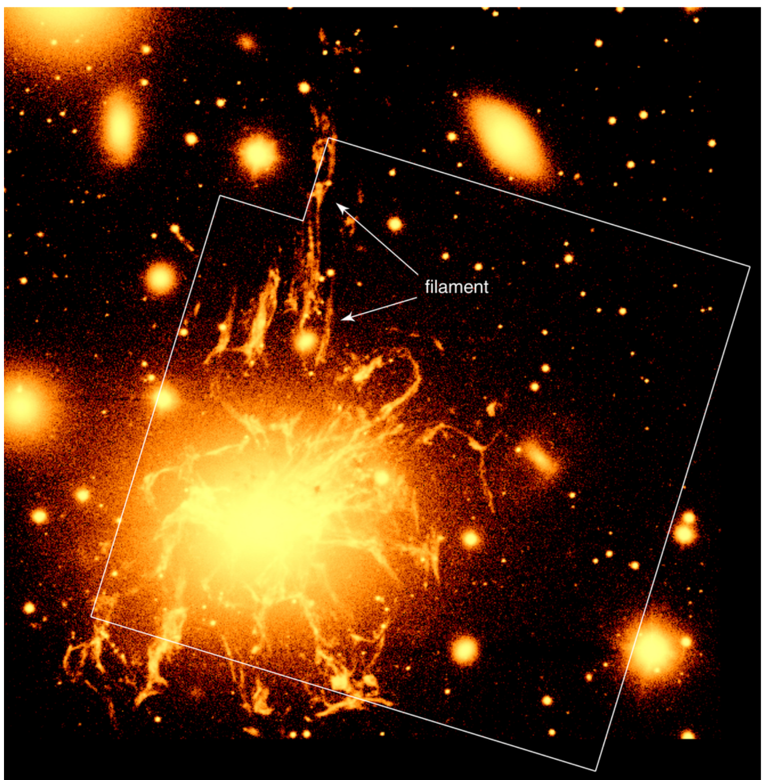

[N16 ext-Fig.7] The SXS field (Obs2 and 3) overlaid on the cold gas nebulosity surrounding NGC 1275.

The image shows Hα emission (Conselice+ 2001). The radial velocity along the long northern filament measured from CO data decreases, south to north (within the SXS field of view), from about +50 km s^{-1} to –65 km s^{-1}. This is similar to the trend seen in the SXS velocity map (Ext-Fig. 6).

Pointing

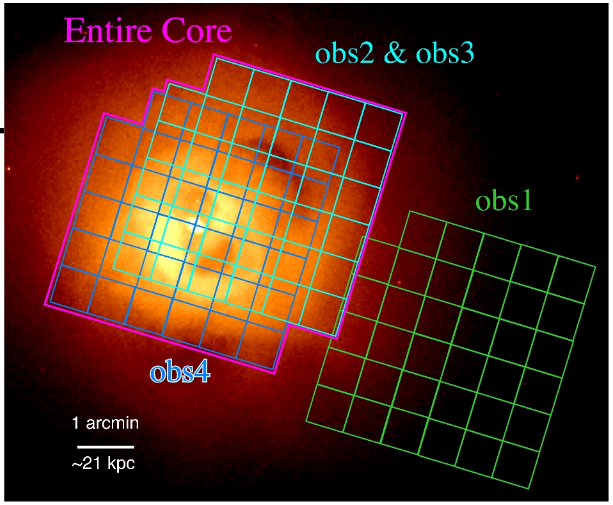

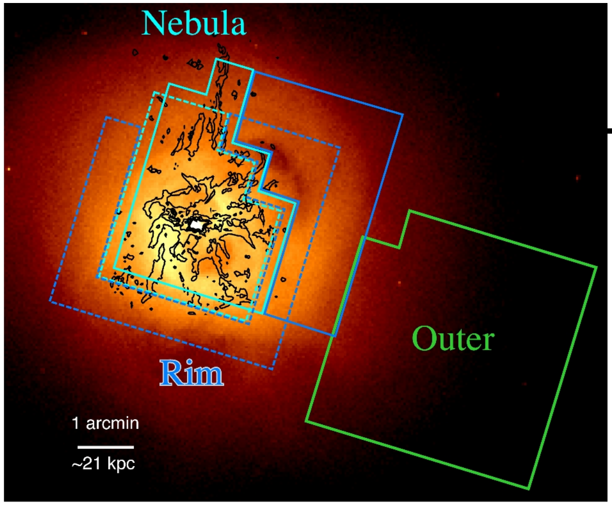

fig.1 (Left) SXS FoVs of the Hitomi observations overlaid on the Chandra X-ray color image in the 1.8–9.0 keV band. The green, cyan, and blue polygons indicate obs1, obs2 and obs3, and obs4, respectively. The 35 square boxes in each FoV correspond to the SXS pixels. The Entire Core region covering the whole obs2/obs3 and obs4 is also shown in magenta. (Right) Analysis regions used in subsection 3.3 overlaid on the same Chandra image. The Hα emission obtained with the WIYN 3.5 m telescope (Conselice et al. 2001) is also shown in the black contours. The cyan, blue, and green polygons correspond to the Nebula, Rim, and Outer regions, respectively. For the Nebula and Rim regions, we used slightly different sky regions between obs2/obs3 and obs4; the regions with solid lines are for obs2/obs3, and those with dashed lines are for obs4

Pointing	Date 2016	Offset	Exposure (ks)
Obs 1	Feb. 24-25	3’ SE	46.6
Obs 2	Feb.25-26	1’ NW	94.1
Obs 3	Mar. 3-5	= 2	137.2
Obs 4	Mar. 6-7	center	43.1

2016 Nature	**The quiescent intracluster medium in the core of the Perseus cluster**	Results (1)
2017 ApJL	Hitomi Constraints on the 3.5 keV Line in the Perseus Galaxy Cluster	
2017 Nature	Solar abundance ratios of the iron-peak elements in the Perseus cluster	
2018 PASJ (**V-paper**)	**Atmospheric gas dynamics in the Perseus cluster observed with Hitomi**	Results (1)
2018 PASJ (RS-paper)	Measurements of resonant scattering in the Perseus Cluster core with Hitomi SXS	Results (1)
2018 PASJ (Temperature-paper)	**Temperature structure in the Perseus cluster core observed with Hitomi**	Results (2)
2018 PASJ (Atomic-paper)	Atomic data and spectral modeling constraints from high-resolution X-ray observations of the Perseus cluster with Hitomi	
2018 PASJ	Hitomi observation of radio galaxy NGC 1275: The first X-ray microcalorimeter spectroscopy of Fe-Kα line emission from an active galactic nucleus	Reynolds, Fukazawa (Morning)

3 Results（1）

X-ray Spectroscopy of
Cluster Dynamics,
Velocity structure

X-ray high energy resolution Spectroscopy

Suzaku (CCD)
ASTRO-H(SXS)

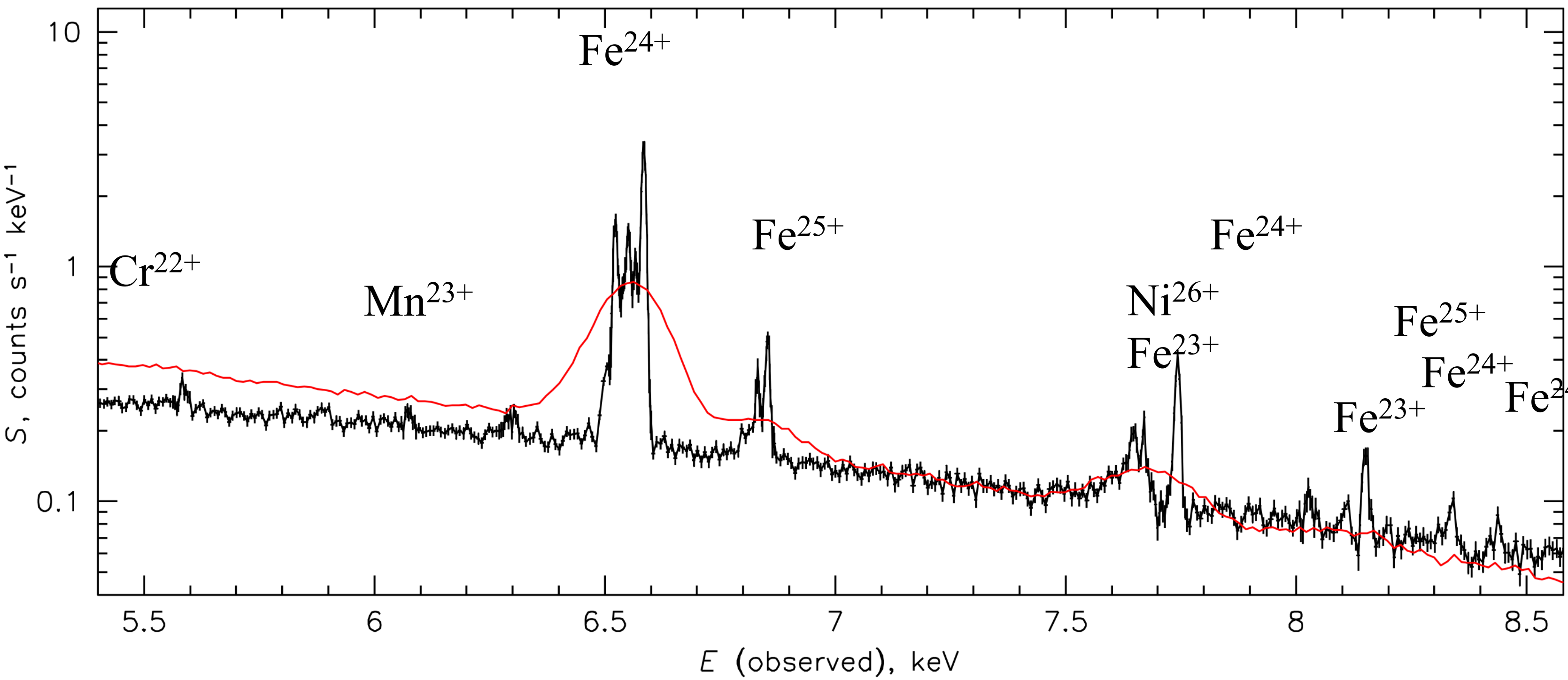

[H16; ext-Fig.1]SXS spectrum of the full field overlaid with a CCD spectrum of the same region. The CCD is the Suzaku X-ray imaging spectrometer (XIS) (red line); the difference in the continuum slope is due to differences in the effective areas of the instruments. The redshift is z=0.01756. Most line transitions are resolved for the 1st time in the cluster plasma.

Line profiles and Velocities

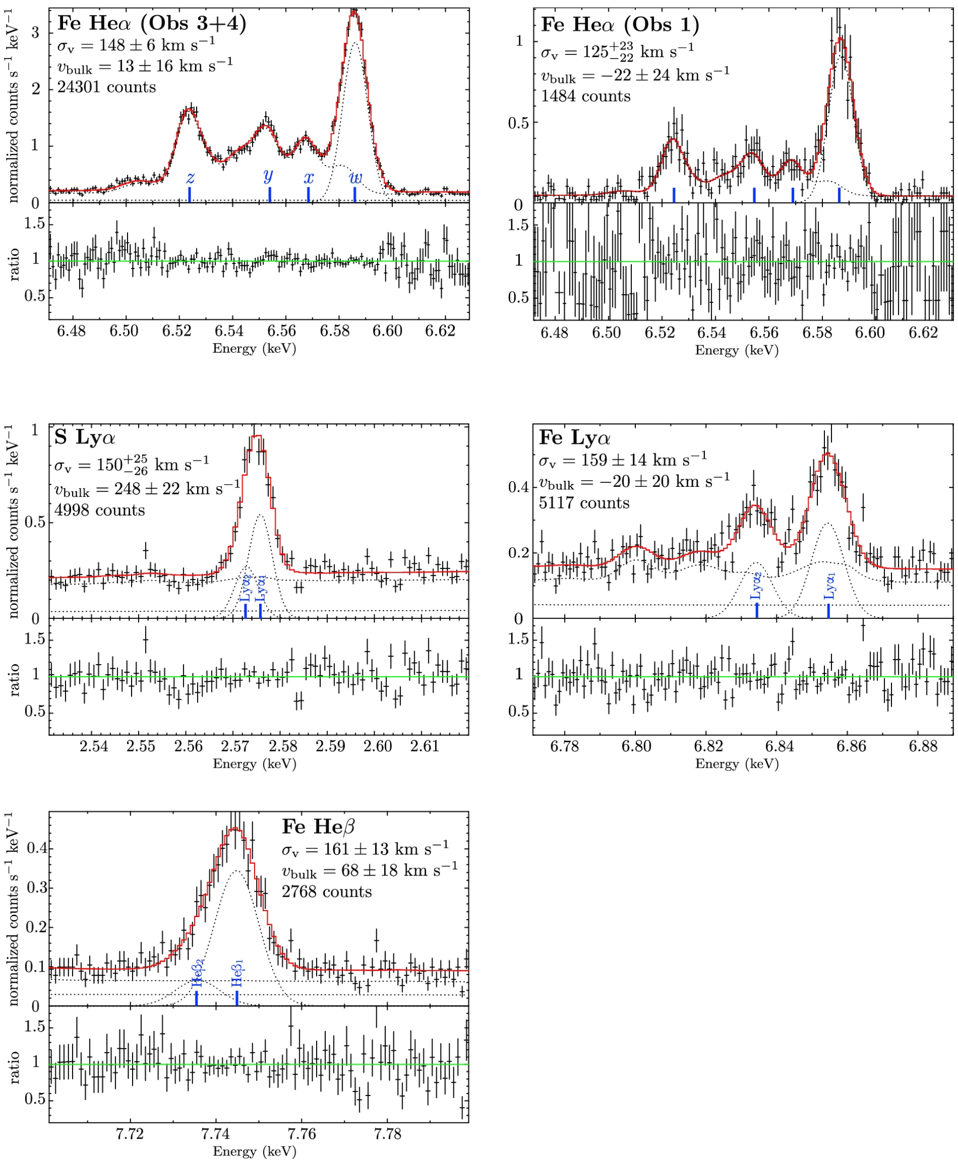

Fig.2&3 Fe He α lines of the full-FOV data of Obs 3 + Obs 4 (left) and Obs 1 (right). The LOS velocity dispersion (σv, w-line excluded), the bulk velocity calculated with respect to the redshift of NGC 1275, and the total number of photons in the displayed energy band are shown in each figure. The red curves are the best-fitting models, and the dotted curves are the spectral constituents, i.e., modified APEC or Gaussian. See the main text for details. The energy bin size is 1 eV or wider for lower count bins. The resonance line (w), the intercombination lines (x and y), and the forbidden line (z) are denoted. The letters are as given in Gabriel (1972).

Line profiles and Velocities

Fig.8 (Upper panels) Data and best-fitting models of Fe Heα w, Lyα1, and Heβ1. The continuum model and the components other than the maim,in line were subtracted. Solid (red) and dashed (green) lines represent the best-fitting Gaussian and Voigtian profiles, respectively. Instrumental broadening with and without thermal broadening are indicated with dotted (blue) and dash–dotted (black) lines. The horizontal axis is the velocity converted from the observed energy, where the line center is set at the origin. The bin size is 1 eV in the energy space, which corresponds to 45.5 km s−1, 43.7 km s−1, and 38.7 km s −1, respectively.

(Lower panels) Ratio spectra of the data to the best-fitting Gaussian models, (left) for Fe Heα w, and (right) for Fe Lyα1 and Heβ1 co-added. Note that the line spread function is not deconvolved from the data.

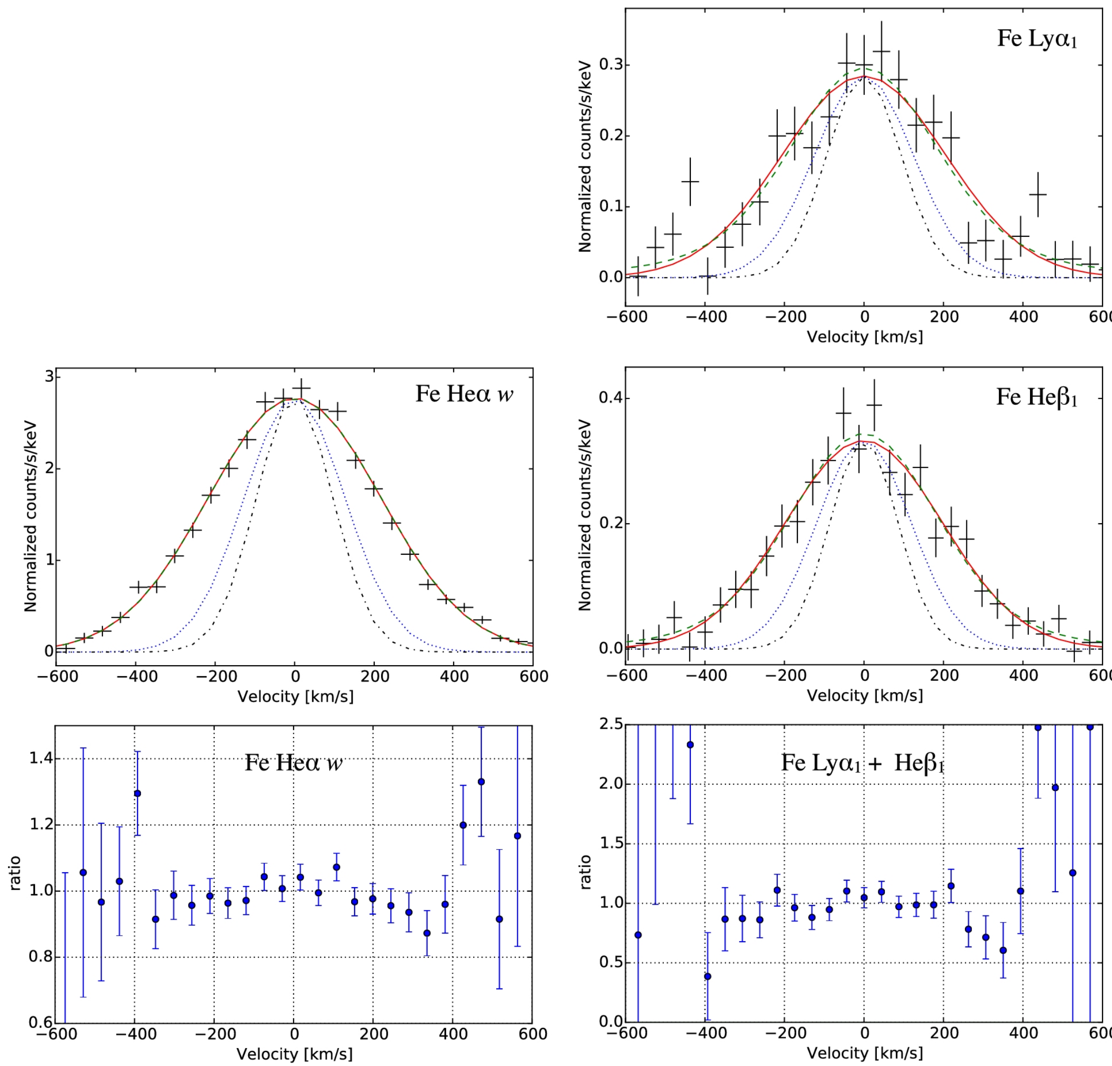

Measurements of Gas dynamics

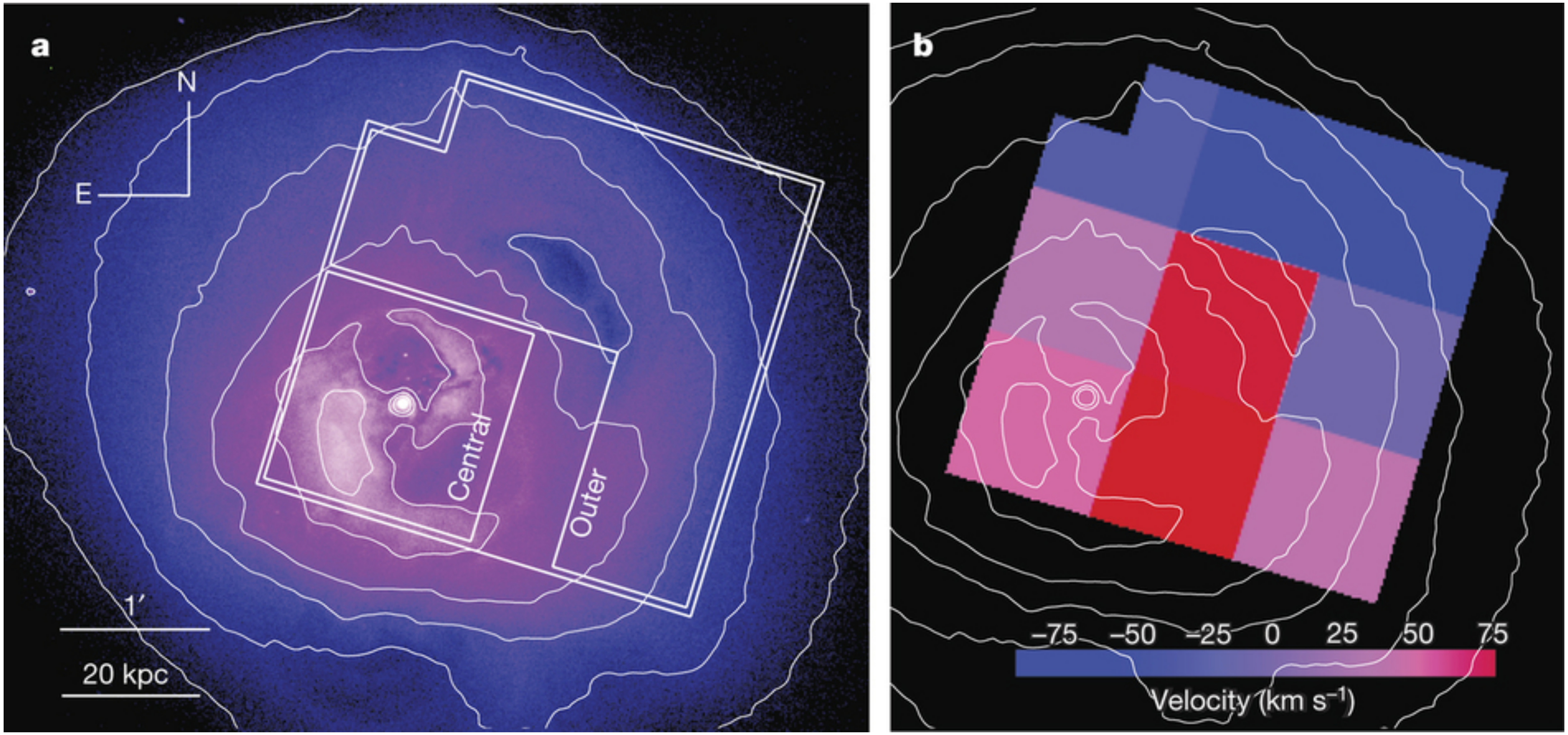

From H16 (fig.3) The region of the Perseus cluster observed by the SXS.

(a) The field of view of the SXS overlaid on a Chandra image. The nucleus of NGC 1275 is seen as the white dot with inner bubbles to the north and south. A buoyant outer bubble lies northwest of the centre of the field. A swirling cold front coincides with the second-most-outer contour. The central and outer regions are marked.

(b) The bulk velocity field across the imaged region. Colours show the difference from the velocity of the central galaxy NGC 1275 (whose redshift is $z = 0.01756$); positive difference means gas receding faster than the galaxy. The 1-arcmin pixels of the map correspond approximately to the angular resolution, but are not entirely independent (see Extended Data Fig. 5).

The calibration uncertainty on velocities in individual pixels and in the overall baseline is 50 km s^{-1} ($\Delta z = 0.00017$).

Velocity Maps

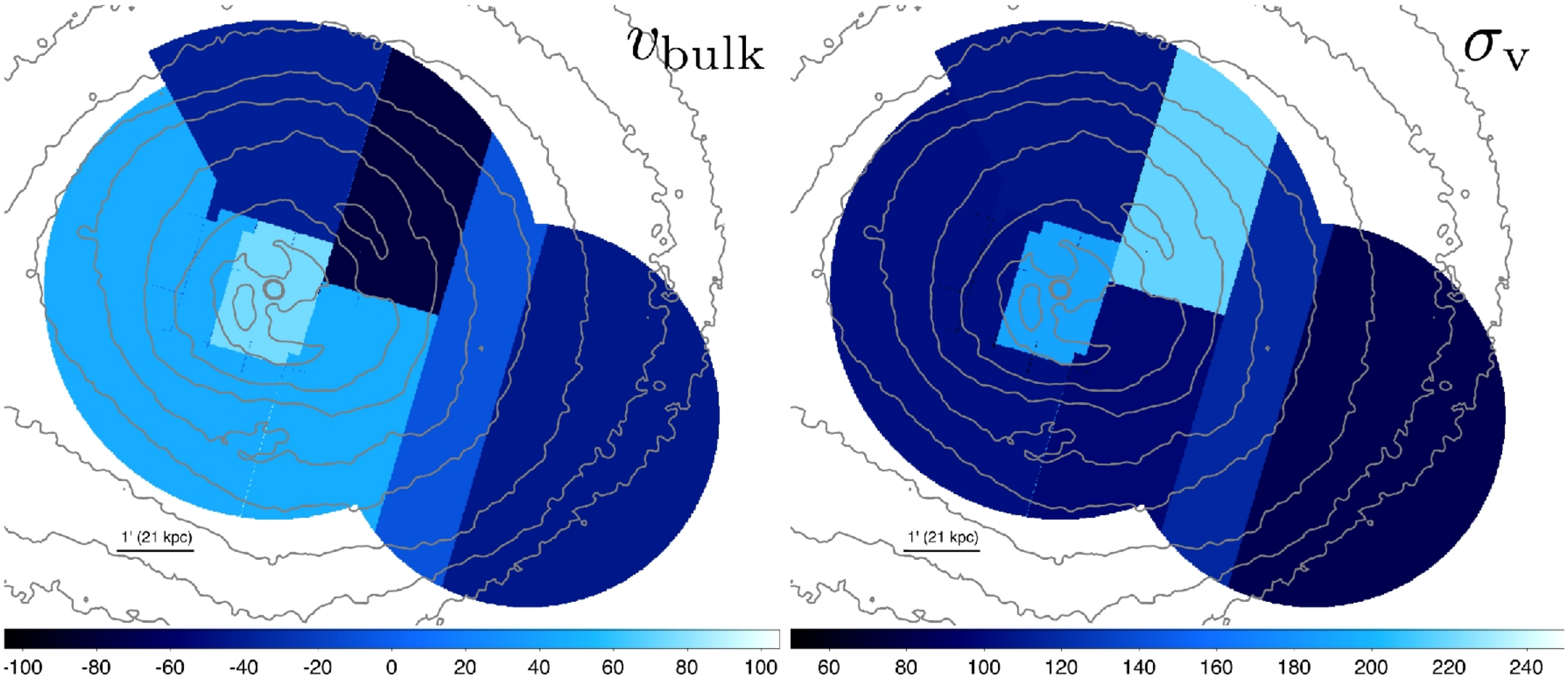

Fig.6 Left: PSF-corrected bulk velocity (vbulk) map with respect to z = 0.017284.
Right: PSF-corrected LOS velocity dispersion (σv) map.
The unit of the values is km s^{-1}. The Chandra X-ray contours are overlaid.

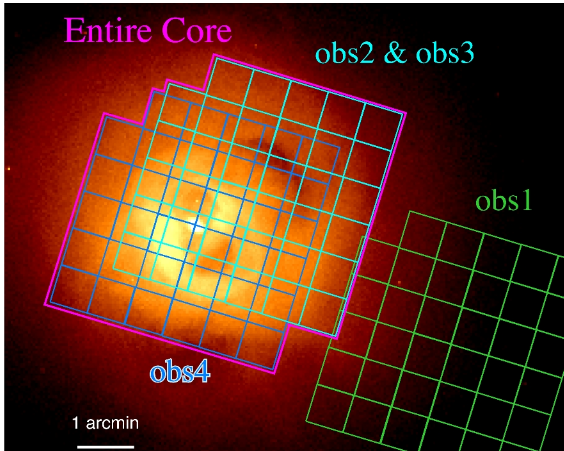

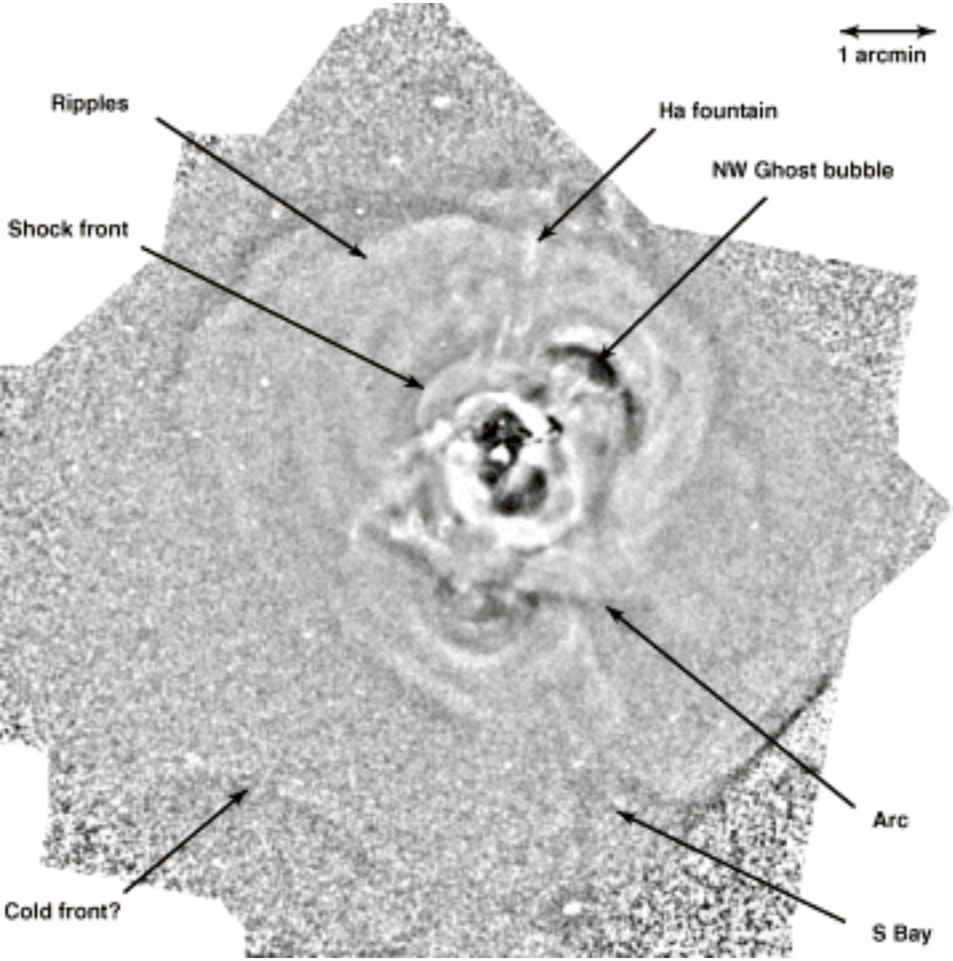

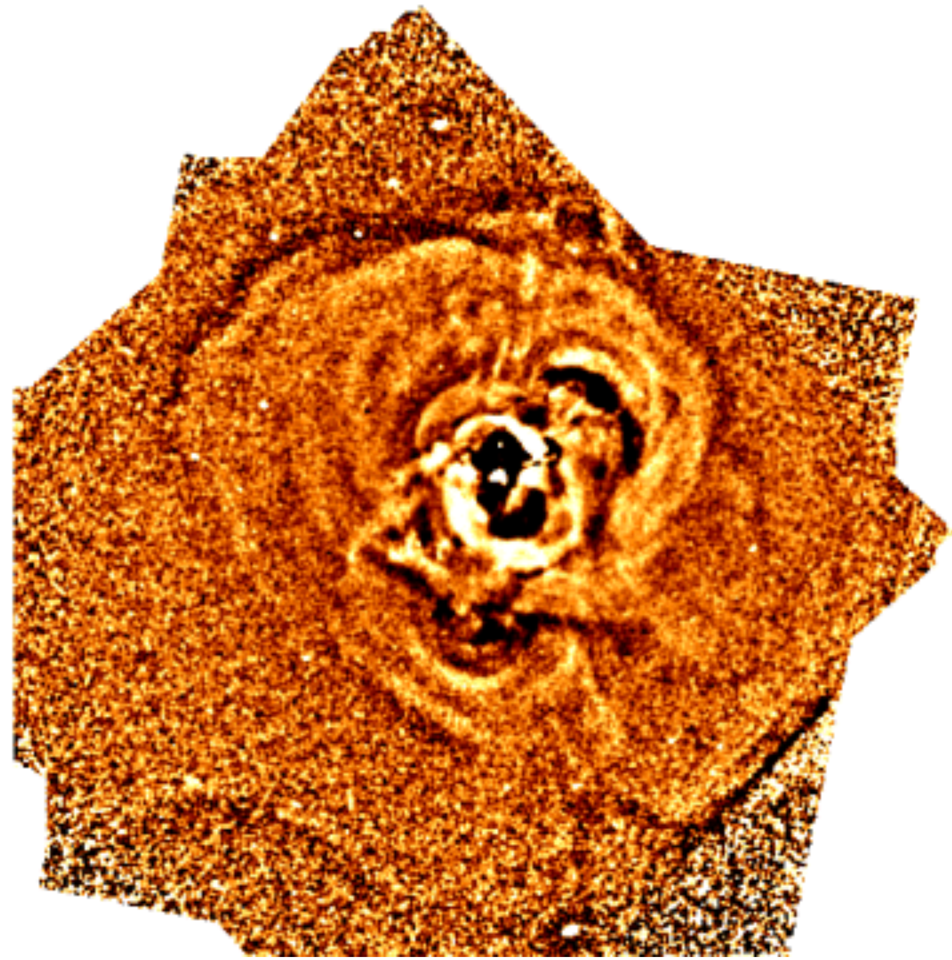

Fabian+ 2006/Fig.2 (unsharp mask Chandra; 11’x 11’)

Discussion: Two peaks in dispersion σv

- The observed peaks in σv appear to indicate that gas motions are driven both
  - (1) at the cluster center by the current AGN inflated bubbles and
  - (2) the buoyantly rising ghost bubbles with diameters of ~25 kpc.
- may indicate that both the current AGN inflated bubbles in the cluster center and the buoyantly rising ghost bubbles are driving gas motions in the Perseus cluster.

Reduction of the Fe-resonance line

❖ Strong resonant transition toward the core: absorbed and re-emitted, τ >1.
❖Column density, oscillator str., Te, Velocity)

(Churazov+ 2004)

centre of the cluster up to a radius of 1 Mpc, $\tau = \int n_{\rm i}\sigma_0\,{\rm d}r$, where $n_{\rm i}$ is the ion concentration and the cross-section for a given ion is

$$\sigma_0 = \frac{\sqrt{\pi}hr_{\rm e}cf}{\Delta E_{\rm D}}, \qquad (3)$$

where

$$\Delta E_{\rm D} = E_0\left(\frac{2kT_{\rm e}}{Am_{\rm p}c^2} + \frac{V_{\rm turb}^2}{c^2}\right)^{1/2}$$

$$= E_0\left[\frac{2kT_{\rm e}}{Am_{\rm p}c^2}(1+1.4AM^2)\right]^{1/2}. \qquad (4)$$

In the above equations E_0 is the energy of a given line, A is the atomic mass of the corresponding element, $m_{\rm p}$ is the proton mass, $V_{\rm turb}$ is the characteristic turbulent velocity, M is the corresponding Mach number, $r_{\rm e}$ is the classical electron radius and f is the oscillator strength of a given atomic transition. The wavelengths and

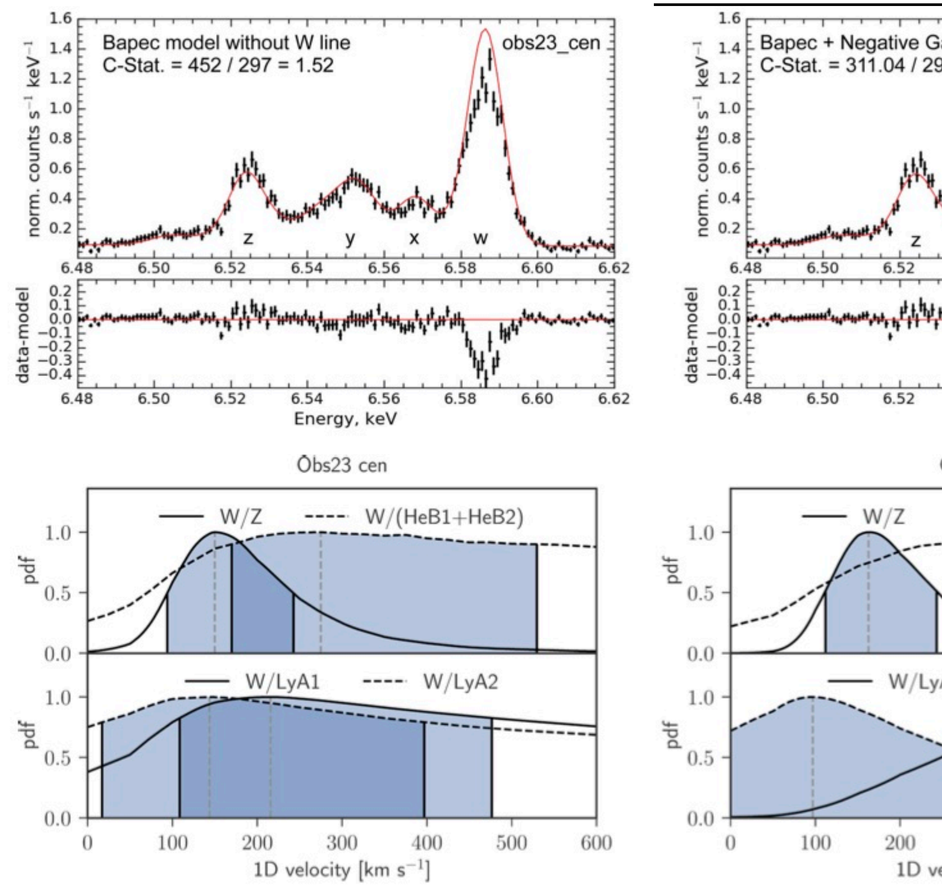

Top: Observed Fe He complex and CIE predicti
Bottom: Velocity probability distributions vs. 1D
from the convolution of the observed line ratios
predicted from numerical simulations of radiativ
Perseus combined with the Hitomi PSF.

Ion kinetic temperature

W in FWHM

$$
\begin{aligned}
W_{\rm inst} &\simeq 5\ {\rm eV}, \\
W_{\rm therm} &= \sqrt{8\ln 2}\left(\frac{kT_{\rm ion}}{m_{\rm ion}c^2}\right)^{1/2} E_{\rm obs}, \\
&= 4.9\ {\rm eV}\left(\frac{kT_{\rm ion}}{5\ {\rm keV}}\right)^{1/2}\left(\frac{m_{\rm ion}}{56\ m_{\rm p}}\right)^{-1/2}\left(\frac{E_{\rm obs}}{6.7{\rm keV}}\right), \\
W_{\rm turb} &= \sqrt{8\ln 2}\left(\frac{v_{\rm turb}}{c}\right) E_{\rm obs}, \\
&= 5.3\ {\rm eV}\left(\frac{v_{\rm turb}}{100\ {\rm km/s}}\right)\left(\frac{E_{\rm obs}}{6.7\ {\rm keV}}\right),
\end{aligned}
$$

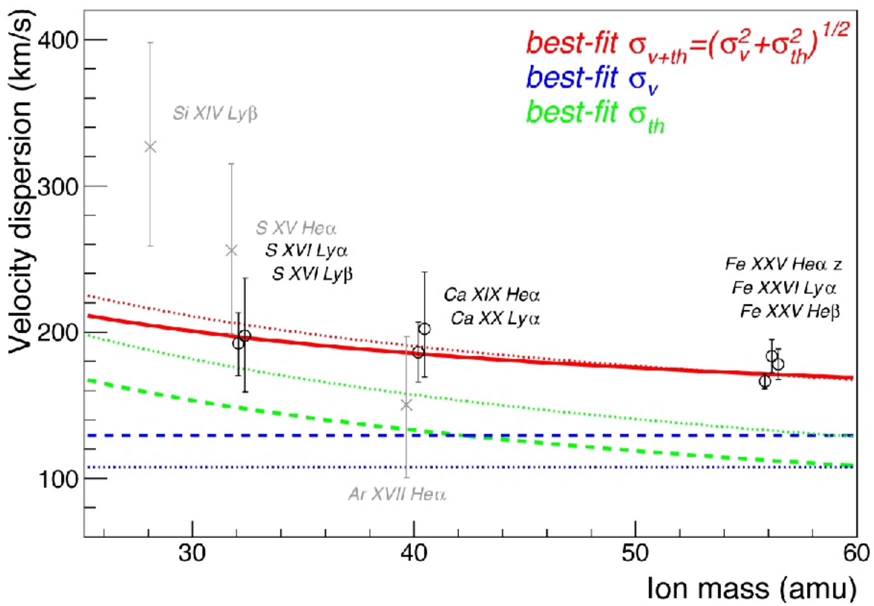

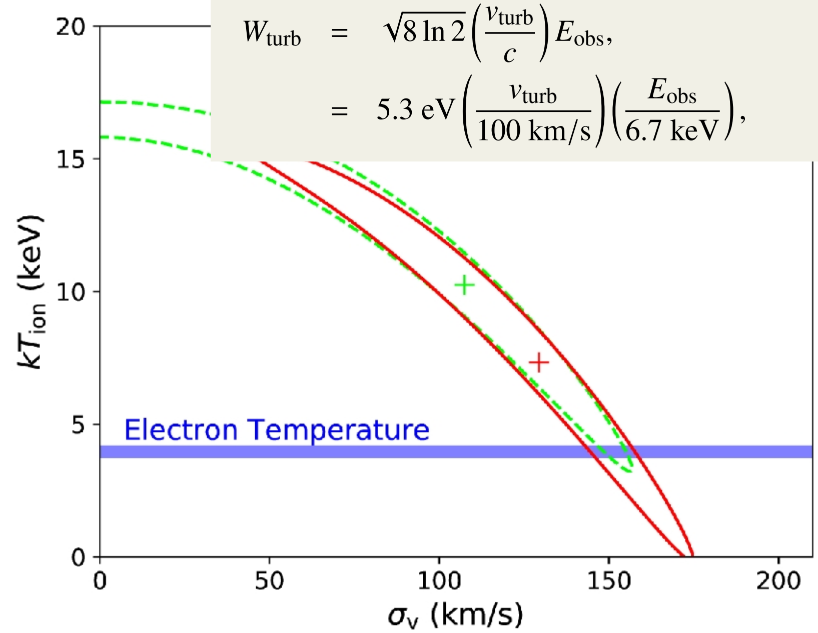

fig.9 Left: **Total velocity dispersion σ_{v+th}** of bright lines as a function of the ion mass in atomic mass units (amu). For clarity, the data points for the same element are slightly shifted horizontally. Black circles and gray crosses denote the lines detected at more than 10σ significance and at 5–10σ significance, respectively. Solid and dashed lines show the best-fitting relation $\sigma_{v+th}=(\sigma^2_{th}+\sigma^2_{v})^{1/2}$ (solid) and its components σ_{th} (dashed) and σ_{v} (dashed) for the >10σ lines. Dotted lines are the best-fitting relation $_{\sigma v+th}$ (red dotted) and its components σth (green dotted) and σv (blue dotted) for the >5σ lines.
Right: **68% confidence regions of kT_{ion} and σ_v** for two parameters of interest ($\Delta\chi^2 = 2.3$) with a plus marking the best-fitting values. Red solid and green dashed contours represent the results for the >10σ and >5σ lines, respectively. For reference, the blue horizontal bar indicates the range of the electron temperature measured in paper T.

Interpretation

- We find the ion temperature to be consistent with the electron temperature.
- Equilibration via Coulomb collisions between the ions and electrons takes place over the timescale.

$$t_{\rm eq} \sim 6 \times 10^6 \ {\rm yr} \left(\frac{n_{\rm e}}{10^{-2} \ {\rm cm}^{-3}} \right)^{-1} \left(\frac{kT}{4 \ {\rm keV}} \right)^{3/2} ,$$

- If the ICM has equilibrated via Coulomb collisions, this equation gives a lower limit to the time elapsed since the last major heat injection.
- This timescale is much shorter than any relevant merger or AGN-related timescales, thus we did not expect to find a discrepancy between $T_{\rm e}$ and $T_{\rm ion}$.
- $T_{\rm ion} \neq T_{\rm ele}$ ⇨ Very recent injection is required.

4 Results (2)

“Temperature structure in the Perseus cluster core observed with Hitomi” (T-Paper)

X-ray Spectral Fitting with

Collisional Ionization Equilibrium (CIE) plasma models

Thermal structure with the CIE fitting

[1] Previous CCD measurements rely on the Bremsstrahlung cut-off shape. Instrumental calibrations (area, background) and multi-T mixture → systematic errors.

[2] Hitomi spectroscopy →

(1) He- and H-like ions ratios → Ionization balance.

(2) Fe He-ion (n=3→1, 2→1 ratio) using excitation rate vs. $T_{electron}$.

[3] A large part of the observed spectra can be described by single temperature CIE (1-CIE) models with T ~ 4 keV (center) and 5 keV (offset). Residual emission above these 1-CIE model are weak.

[4] Model uncertainties (APEC vs. SPEC) limit precise constrains to identify small level of deviation from the CIE state. See the Atomic-paper.

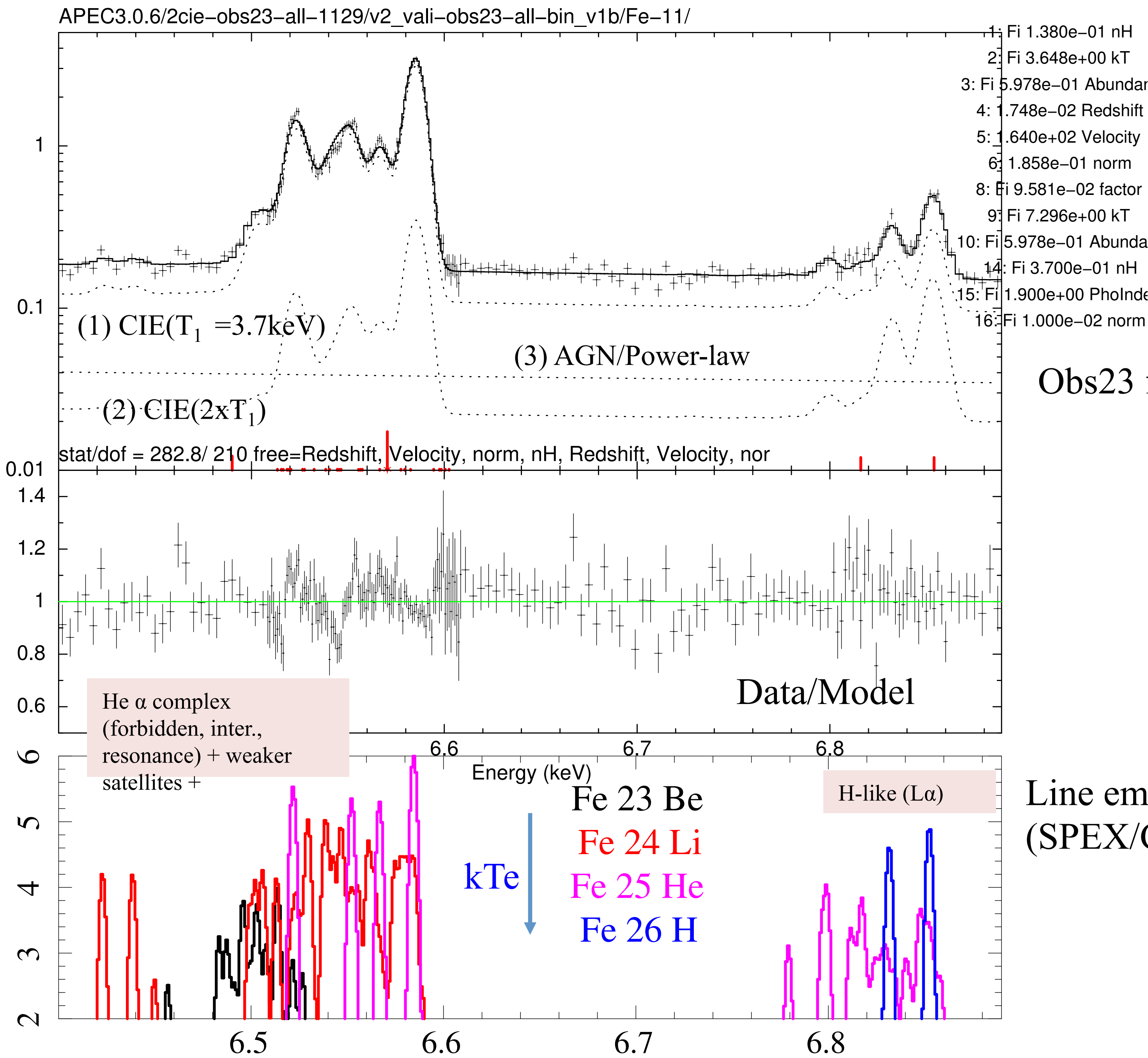

Fitting parameters. Free or Fixed.

Obs23 full-fov

Line emission model (SPEX/CIE/4keV)

Line ratio spectroscopy

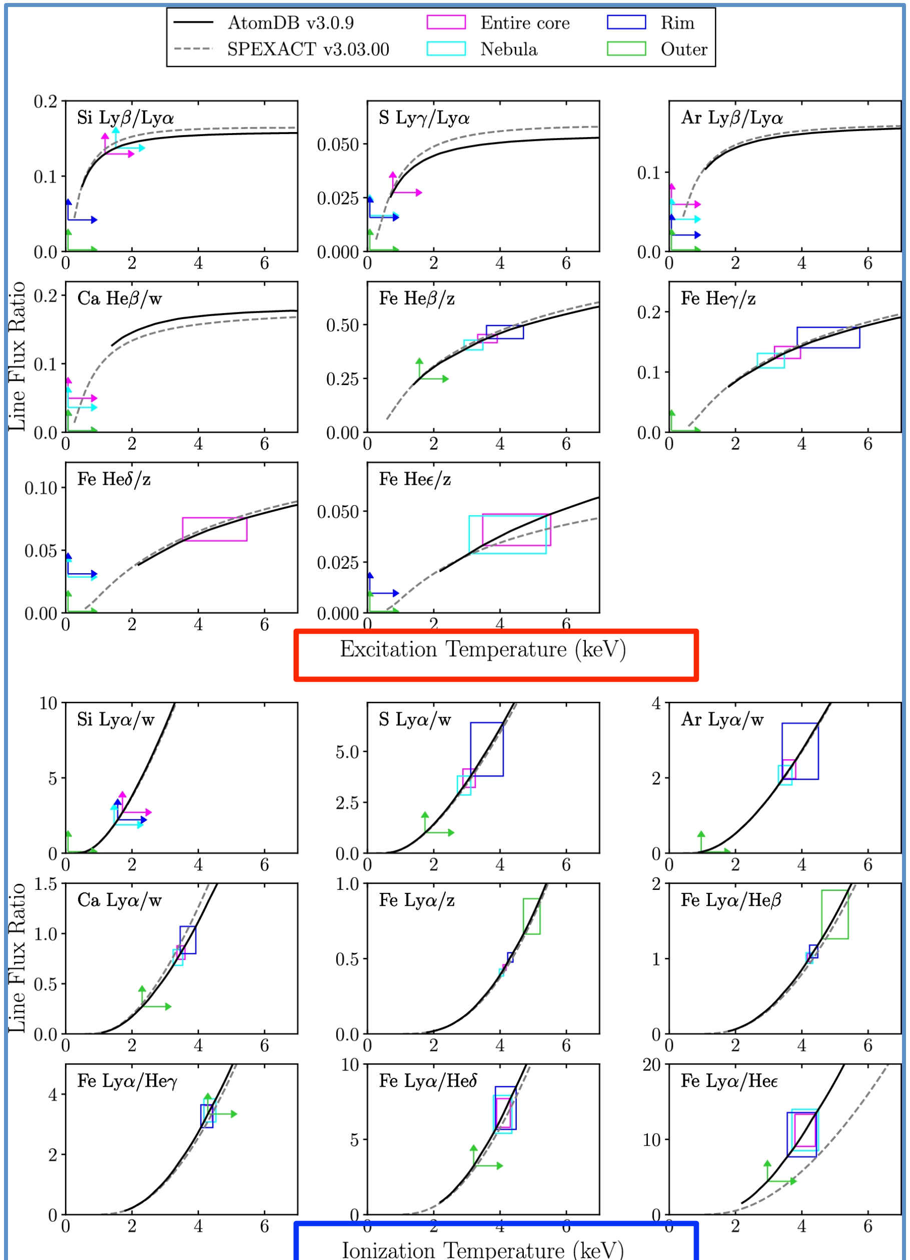

fig.4 Upper panels: the flux ratios of the emission lines as a function of the excitation temperature, calculated from AtomDB (black solid curve) and SPEXACT (gray-dashed curve) assuming a single-temperature CIE plasma. The lines used in the calculations are denoted in each panel. The color boxes show the ranges of the observed line ratios and the corresponding AtomDB temperatures at the 1σ confidence level. Magenta, blue, cyan, and green correspond to the Entire Core, Rim, Nebula, and Outer regions, respectively. When the ranges of the statistical errors of the observed line ratios are outside the models, 3σ lower limits are shown instead by the color arrows.
Lower panels are the same as the upper panels, but for the ionization temperature.

fig.5 Excitation temperatures and ionization temperatures derived from individual line ratios in (a) the Entire Core, (b) Nebula, (c) Rim, and (d) Outer regions. Cyan, green, orange, pink, and purple indicate Si, S, Ar, Ca, and Fe, respectively. The results based on AtomDB and SPEXACT are shown by the solid and dotted lines, respectively. The horizontal dot-dashed lines show the best-fit kTline of the modified-1T model described in

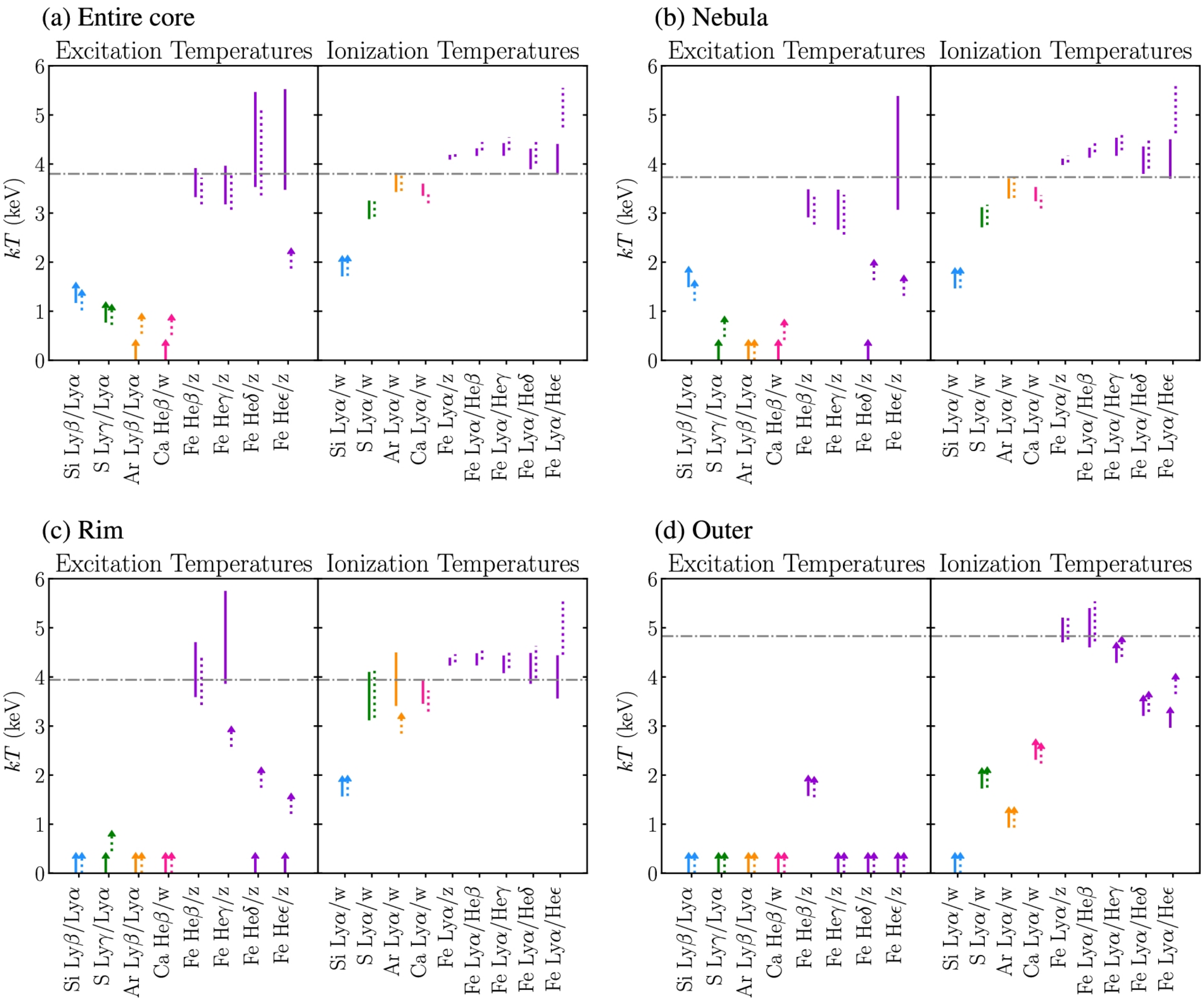

Spectral fits

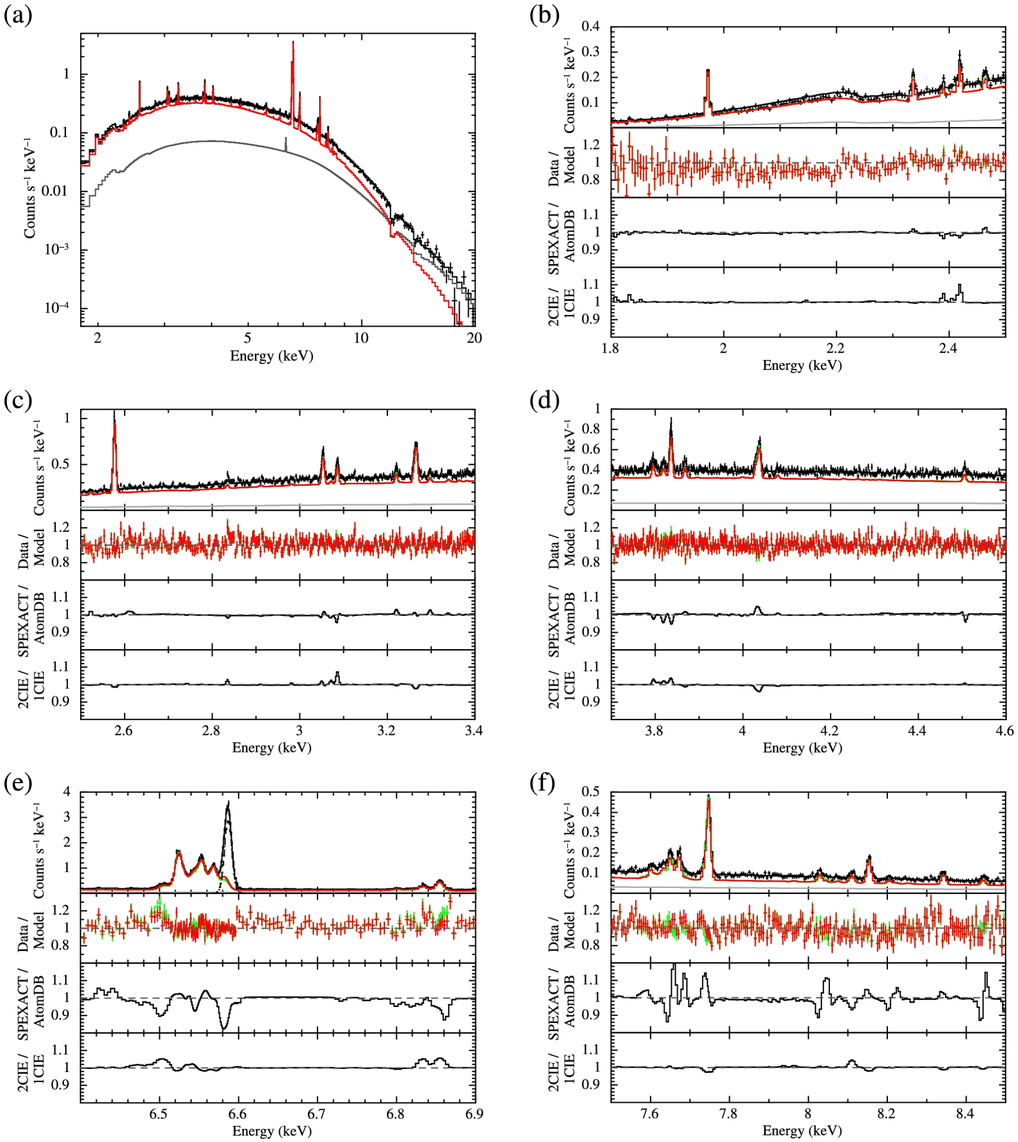

fig.6 Spectra in **the Entire Core region** fitted with the modified-1CIE model. The entire energy band of 1.8–20.0 keV is shown in (a), and narrower energy are shown in panels (b)–(f). The black solid curve is the total model flux, and the red and gray curves indicate the ICM component based on AtomDB and the AGN component, respectively; panels (b)–(f) include the green lines, indicating the ICM component based on SPEXACT. The panel (e), covering the 6.4–6.9 keV band, also shows the Gaussian (black-dashed curve) which substitutes Fe XXV w in the plasma model. All the spectra are rebinned after the fitting just for display purposes. The second subpanels in (b)–(f) are the ratios of the data to the models of AtomDB (red) and SPEXACT (green). The third subpanels in (b)–(f) are comparisons of SPEXACT and AtomDB in the modified-1CIE model. The bottom subpanels in (b)–(f) show the ratio of the 2CIE model to the modified-1CIE model based on AtomDB.

Thermal structure

Table 4. Best-fit parameters for the Entire Core region.

Model/parameter	AtomDB v3.0.9	SPEXACT v3.03.00
1CIE model		
kT_{1CIE} (keV)	$3.95^{+0.01}_{-0.01}$	$3.94^{+0.01}_{-0.01}$
N (10^{12} cm^{-5})	$23.20^{+0.05}_{-0.05}$	$22.78^{+0.04}_{-0.04}$
C-statistics/dof	13123.6/12979	13181.7/12979
Modified-1CIE model		
kT_{cont} (keV)	$4.01^{+0.01}_{-0.01}$	$3.95^{+0.01}_{-0.01}$
kT_{line} (keV)	$3.80^{+0.02}_{-0.02}$	$3.89^{+0.02}_{-0.02}$
N (10^{12} cm^{-5})	$22.77^{+0.04}_{-0.04}$	$22.67^{+0.05}_{-0.05}$
C-statistics/dof	13085.9/12978	13178.7/12978
2CIE model (modified CIE + CIE)		
kT_{cont1} (keV)	$3.66^{+0.01}_{-0.02}$	$3.40^{+0.02}_{-0.01}$
kT_{line1} (keV)	$3.06^{+0.04}_{-0.03}$	$2.92^{+0.03}_{-0.03}$
kT_2 (keV)	$4.51^{+0.02}_{-0.03}$	$4.73^{+0.02}_{-0.02}$
N_1 (10^{12} cm^{-5})	$12.98^{+0.05}_{-0.05}$	$13.27^{+0.13}_{-0.09}$
N_2 (10^{12} cm^{-5})	$9.71^{+0.06}_{-0.05}$	$9.45^{+0.07}_{-0.05}$
C-statistics/dof	13058.5/12976	13093.9/12976
Power-law DEM model		
α	$10.92^{+0.11}_{-0.11}$	$4.68^{+0.03}_{-0.03}$
kT_{max} (keV)	$4.01^{+0.06}_{-0.01}$	$4.29^{+0.01}_{-0.01}$
N (10^{12} cm^{-5})	$21.38^{+0.24}_{-0.24}$	$15.39^{+0.04}_{-0.04}$
C-statistics/dof	13123.4/12978	13147.6/12978
Gaussian DEM model		
kT_{mean} (keV)	$3.94^{+0.01}_{-0.01}$	$3.89^{+0.01}_{-0.01}$
σ (keV)	$0.60^{+0.08}_{-0.11}$	$1.01^{+0.05}_{-0.05}$
N (10^{12} cm^{-5})	$11.65^{+0.02}_{-0.02}$	$11.67^{+0.03}_{-0.03}$
C-statistics/dof	13121.1/12978	13138.7/12978

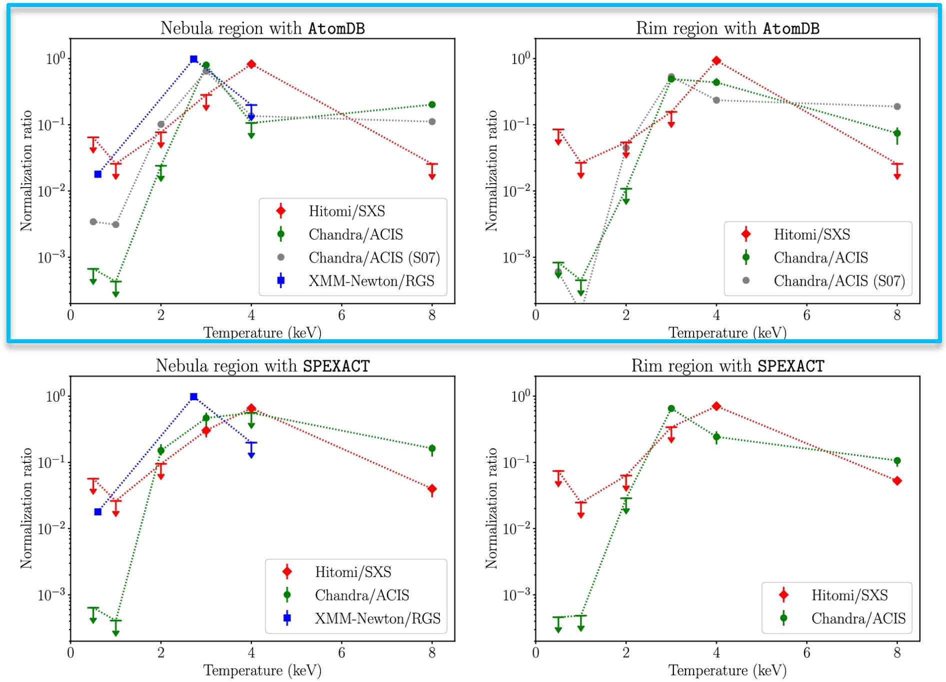

fig.10 Normalization ratios of each temperature component derived from the multi-temperature models. The top row is the results from AtomDB and the bottom row is those from SPEXACT. The left- and right-hand columns correspond to the Nebula and Rim regions, respectively. The red diamonds are Hitomi/SXS, the black circles are Chandra/ACIS, the gray circles are Chandra/ACIS of Sanders and Fabian (2007), and the blue squares are XMM-Newton/RGS. The results of XMM-Newton/RGS are shown only in the Nebula region because the RGS data does not cover the Rim region.

5. Discussion

(1) Gas and Steller *absolute* velocities

- V(center) = 75 ± 25 (stat.) km/s, relative to a new redshift of NGC 1275 (z=0.017284 ±0.00005).
- Systematic error of the SXS energy scale (See A.2.1)
  - < 0.3 eV (Obs3/4)~ 15 km/s @ 7keV
  - 0.5 eV (pixel-to-pixel)
- consistent with No redshift → Gas and stars stay together at the bottom of the cluster. No peculiar velocity of the BCG.
- NGC 1275 hosts a giant (80kpc wide) molecular nebula seen in CO and Hα data whose mass dominates the total gas mass out to a 15 kpc radius. The velocities of that gas are consistent with the trend of the SXS bulk shear, suggesting that the molecular gas moves together with the hot plasma.

(2) Large or small scale motions ?

- During the process of hierarchical structure formation, turbulent gas motions are driven on Mpc scales by mergers and accretion flows (their kinetic energy into turbulence).
- These turbulent motions then cascade down from the driving scales to dissipative scales, heating the plasma, accelerating cosmic-rays, and amplifying the magnetic fields.
- In the Perseus cluster, turbulence is also likely to contribute to powering the radio emission of the mini-halo.

- The observed velocity dispersion is dominated by small-scale motions. The turbulence in the Perseus core is driven primarily on scales smaller than ~100 kpc.
  1. The lack of observed radial increase in and the relative uniformity of dispersion σv.
  2. The superposition of large-scale motions over the LOS within our extraction area should therefore lead to non-Gaussian features in the observed line shapes. The lack of evidence for non-Gaussian line shapes in the spectral lines extracted over a spatial scale of ~100 kpc.

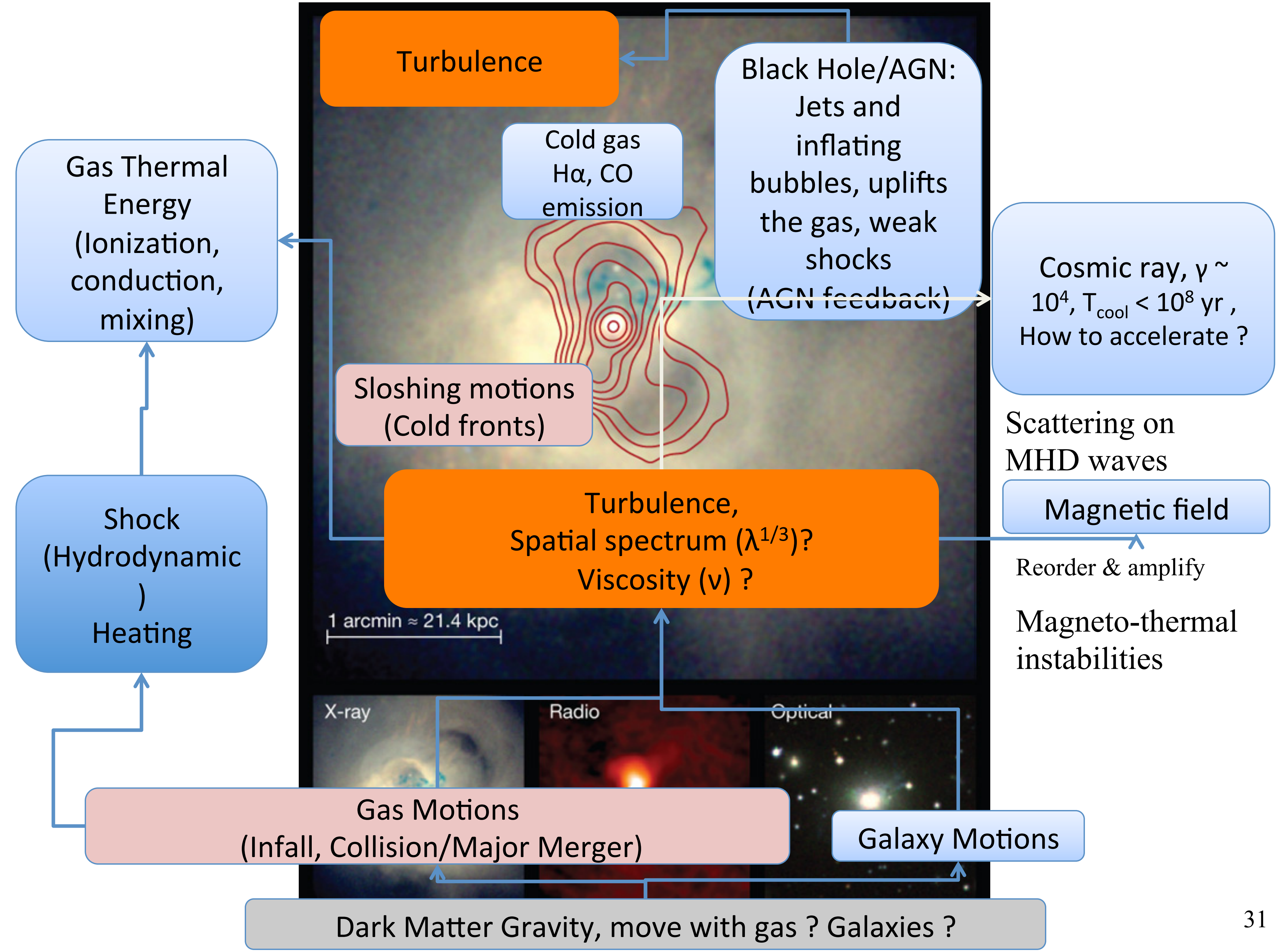

Turbulence
Black Hole/AGN: Jets and inflating bubbles, uplifts the gas, weak shocks (AGN feedback)
Cold gas Hα, CO emission
Gas Thermal Energy (Ionization, conduction, mixing)
Cosmic ray, γ ~ 10^4, T_cool < 10^8 yr , How to accelerate ?
Sloshing motions (Cold fronts)
Scattering on MHD waves
Magnetic field
Shock (Hydrodynamic) Heating
Turbulence, Spatial spectrum (λ^1/3)? Viscosity (ν) ?
Reorder & amplify
1 arcmin ≈ 21.4 kpc
Magneto-thermal instabilities
X-ray
Radio
Optical
Gas Motions (Infall, Collision/Major Merger)
Galaxy Motions
Dark Matter Gravity, move with gas ? Galaxies ?

(3) Cooling and heating balance and energy transport

- The gas in the core of galaxy clusters appears to be in an approximate global thermal balance, which is likely maintained by several heating and energy transport mechanisms taking place simultaneously.
- One possible heat source is the central AGN.
- A feedback loop, where the hot ICM cools and accretes on to the central AGN, leading to the formation of jets which heat the surrounding gas, lowering the accretion rate, reducing the feedback, until the accretion eventually builds up again (e.g.McNamara & Nulsen 2007; Fabian 2012).
- How to transport energy from the bubbles to the ICM ?
  - Turbulence generated in situ by bubble-driven gravity waves oscillating within the gas (e.g., Churazov et al. 2001; Reynolds et al. 2015;
  - Bubble-generated sound waves (Fabian et al. 2003; Fujita & Suzuki 2005; Sanders & Fabian 2007; Fabian 2017),
  - Cosmic ray streaming and mixing (e.g., Loewenstein et al. 1991; Guo & Oh 2008; Fujita & Ohira 20112017)
  - Mixing of the bubbles (e.g., Hillel & Soker 2016, 2017).

Turbulence and dissipation heating

- The ratio of turbulent pressure to thermal pressure in the ICM is low at 4%. Such low-velocity turbulence cannot spread far (<10 kpc) across the cooling core during the fraction (4%) of the cooling time in which it must be replenished with v < observed dispersion or bulk ones.
- The turbulent-dissipation mechanism requires that turbulence be generated in situ throughout the core. Another process is needed to transport energy from the heat source (e.g. Fabian+ 2017).
- A low level of turbulent pressure measured for the core region of a cluster may imply that turbulence is difficult to generate and/or easy to damp.
- If the observed dispersion is interpreted as a certain type of turbulence it is in agreement with the level inferred from X-ray surface brightness fluctuations (Zhuraleve+ 2014).

(4) Kinetic pressure support

- If the observed velocity dispersion is due to isotropic turbulence, the inferred range of σ v ~ 100–200 km s−1 corresponds to 2%–6% of the thermal pressure support of the gas with *kT* = 4 keV.
- The large-scale bulk motion will also contribute to the total kinetic energy.
  - $Cs = \gamma kT/\mu m_p = 1030(kT/4\text{ keV})^{1/2}\text{ km s}^{-1}$

$$\frac{\epsilon_{\mathrm{kin}}}{\epsilon_{\mathrm{therm}}} = \frac{\mu m_{\mathrm{p}}(3\sigma_{\mathrm{v}}^2 + v_{\mathrm{bulk}}^2)}{3kT} \sim 0.02\text{–}0.07,$$

- If the velocity dispersion is mostly sloshing-induced, we might be underestimating the kinetic energy density. This would change the upper bound of the kinetic to thermal pressure ratio to 0.11–0.13.
- The low level of turbulence is encouraging for total mass measurements and for cluster cosmology.

Summary（1: Velocity part）

I. Developed and launched an X-ray observatory, *Hitomi*.
II. Observed the Perseus core, the X-ray brightest extragalactic extended source.
III. Resolved and measured the line widths of He-like and H-like ions of Si, S, Ar, Ca, and Fe in the hot ICM for the first time.
IV. The line-of-sight velocity dispersion (σ_v) of the hot gas is mostly low and uniform.
   I. The velocity dispersion reaches maxima of ~ 200 km s^{-1} toward the central AGN and toward the AGN-inflated northwestern "ghost" bubble.
   II. Elsewhere within the observed region, σ_v appears nearly uniform at ~100 km s^{-1} .
V. Detect a large-scale bulk velocity gradient of ~100 km s^{-1} across the core.
VI. The mean redshift of the hot atmosphere is consistent with that of the stars of the central galaxy NGC 1275.
VII. The shapes of well-resolved optically thin emission lines are consistent with a Gaussian → the observed σ_v and its driving scales < 100 kpc.
VIII. The kinetic pressure support < 10 % of the thermal one.
IX. The widths of the lines formed from various elements → the 1st direct constraints on the thermal motions of the ions in the hot ICM; Electrons and ions are in equilibrium.
X. Detected distortions of the Fe He resonance line flux, shape, and distance dependence, consistent with the resonant scattering in the core. → independent constrains on the gas motions.

Summary（2:Temperature, Metal, Models）

- Not only fine structures of K-shell lines in He-like ions, but also transitions from higher principal quantum numbers were clearly resolved from Si through Fe.
  - temperature diagnostics using the line ratios of Si, S, Ar, Ca,
  - The 1st direct measurement of the excitation temperature and ionization state.
- The observed spectrum is roughly reproduced by a single-temperature thermal plasma model in collisional ionization equilibrium, but detailed line-ratio diagnostics reveal slight deviations from this approximation.
- The best-fit two-temperature models suggest a combination of 3 and 5 keV gas. The observed small deviations from a single-temperature model → the effects of projecting the radial temperature gradient.
- Si, S, Ar, Ca, Cr, Mn, Ni to Fe ratios are close to the Solar pattern. → SN Ia/Core-collapsed ratios, nature of SN Ia progenitor types.
- High quality Perseus spectra vs. ATOMDB and SPEX models.
  - Success: reasonable fits to the broad-band spectrum with consistent results from the two models.
  - Challenges: systematic model uncertainties around strong lines (e.g. Fe He complex).

Future X-ray Spectroscopy Missions

- X-ray Astronomy Recovery Mission (XARM)
  - to resume the X-ray Astrophysics that should be achieved by Hitomi
  - JAXA is preparing to start a project in collaboration with NASA and other partners.
  - Minimum Instruments (Calorimeter +CCD)
  - Launch is planed in 2021FY.
- Athena (2028~)

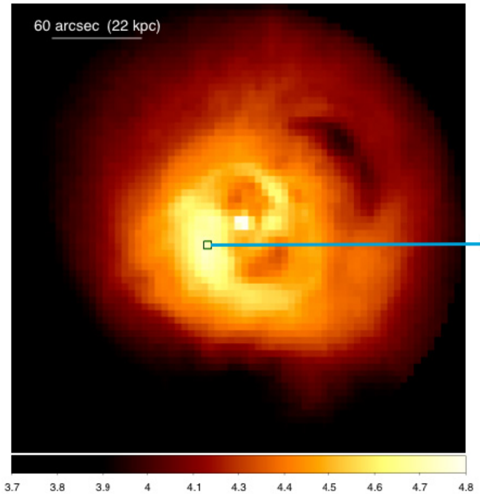

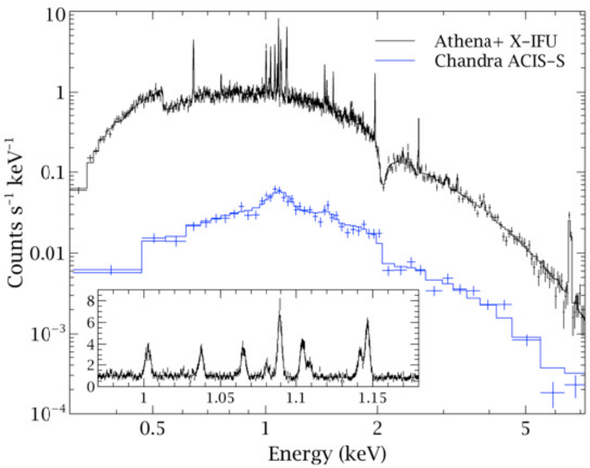

From the Athena web page J.H. Croston, J.S. Sanders, et al.

backup

Line emissicity

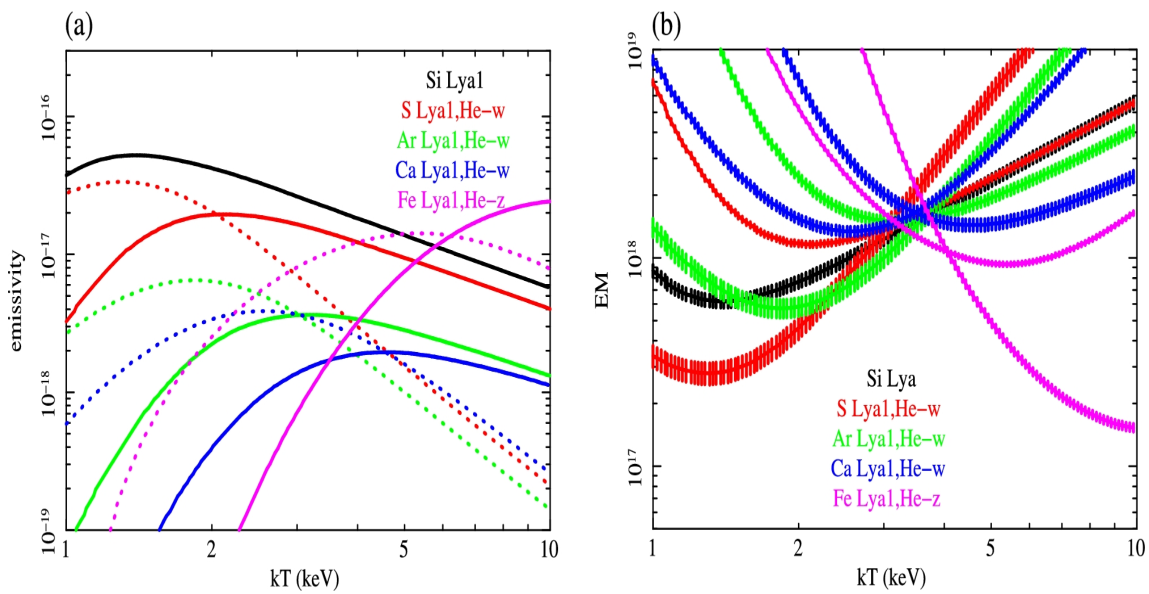

fig.14(a) Line emissivities of strong transitions from AtomDB for a given emission measure and metal abundances. The solid and dashed lines show H-like and He-like transitions, respectively. (b) Emission measure limits calculated from the AtomDB-CIE model and the observed fluxes from the Entire Core region.

Line profile: Gaussian ?

- Observed bright transition lines, Fe He-resonance(w), Lyα, Heβ are consistent with a Gaussian, little deviation.
- No clear spatial variation.
- → velocity distribution within 60kpc is relaxed and smooth.
- → No large scale motions effect on the line profile.
- → Major (large scale) merger was long ago and current turbulence driving scale < 60 kpc.

Nebula/
Center

Rim/
Outer

Line profile Gaussian ?
Predictions (Sunyaev+ 2003)

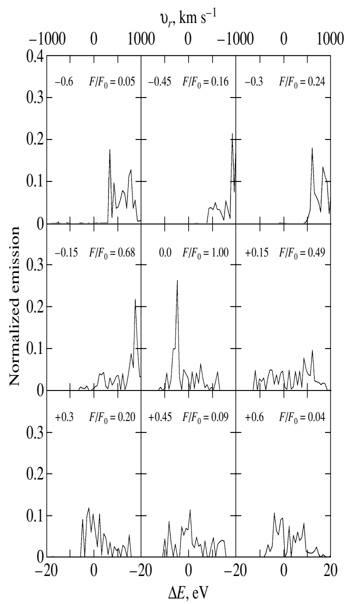

Fig. 4. The normalized X-ray emission versus Doppler shift in eV along nine lines of sight through the simulated X-ray cluster. The corresponding radial velocities are given at the top of the plot. The impact parameter in Mpc for each l.o.s. is given at upper left in each panel. The flux F in units of the central flux F_0 is given at upper right in each panel.

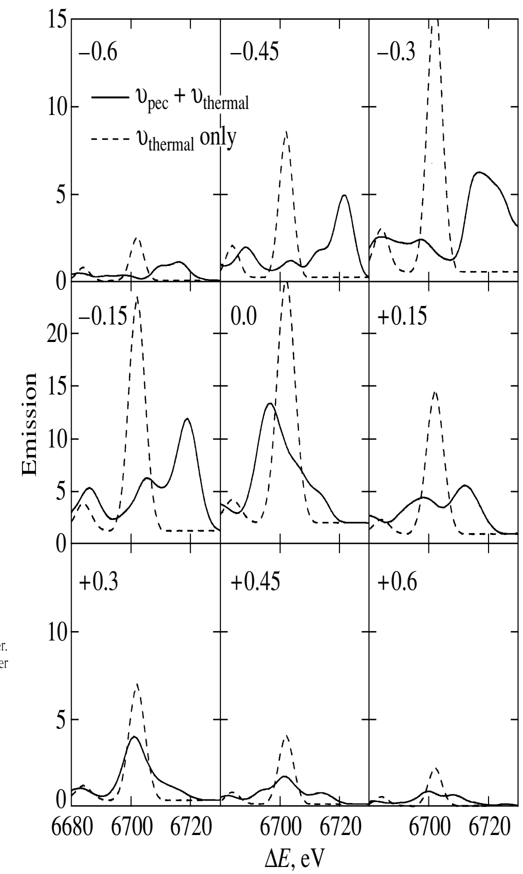

Fig. 5. Synthetic Fe line spectra along nine lines of sight through the simulated X-ray cluster. The dashed lines are computed assuming thermal broadening only, whereas the solid lines include both thermal broadening and Doppler shift.

A2256, X-ray bright, double peaked merging cluster

galaxy radial velocities Berrington et al. 2002

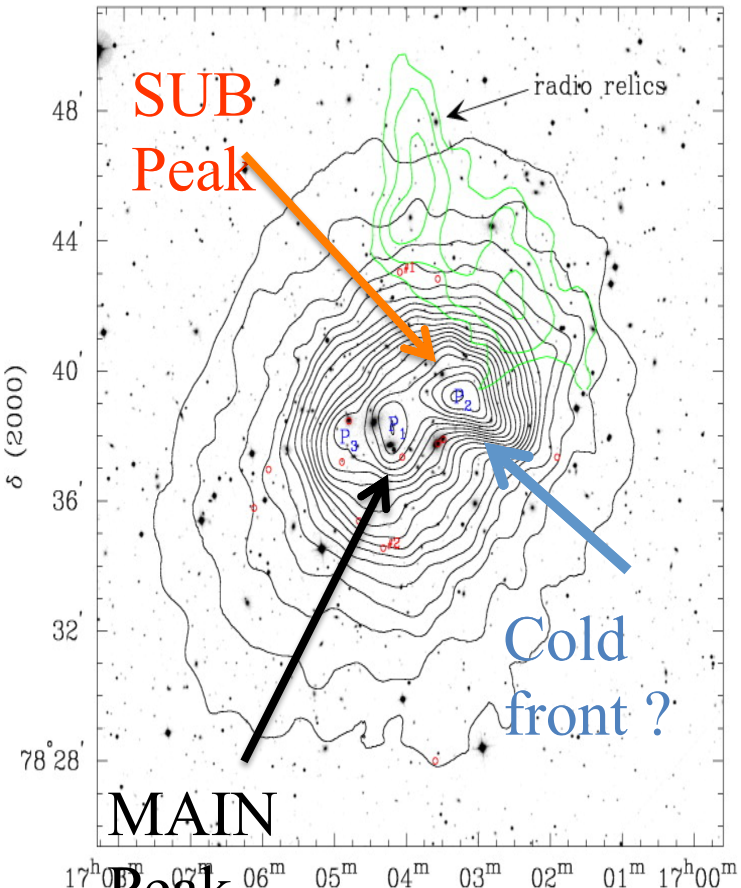

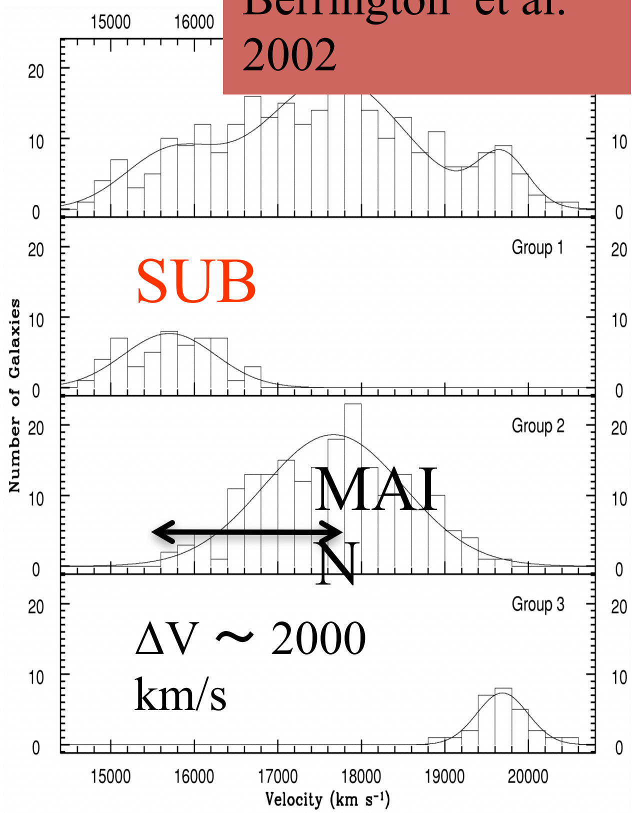

Chandra X-ray Contour + galaxy image (Sun+ 2002). See also Briel+ 1991

Radio: a diffuse halo, relics, and tailed emission from galaxies → dynamically young (e.g. Rottgering+ 1994)

Discovery of Gas Bulk motion in A2256 with *Suzaku* (Tamura+ 2011)

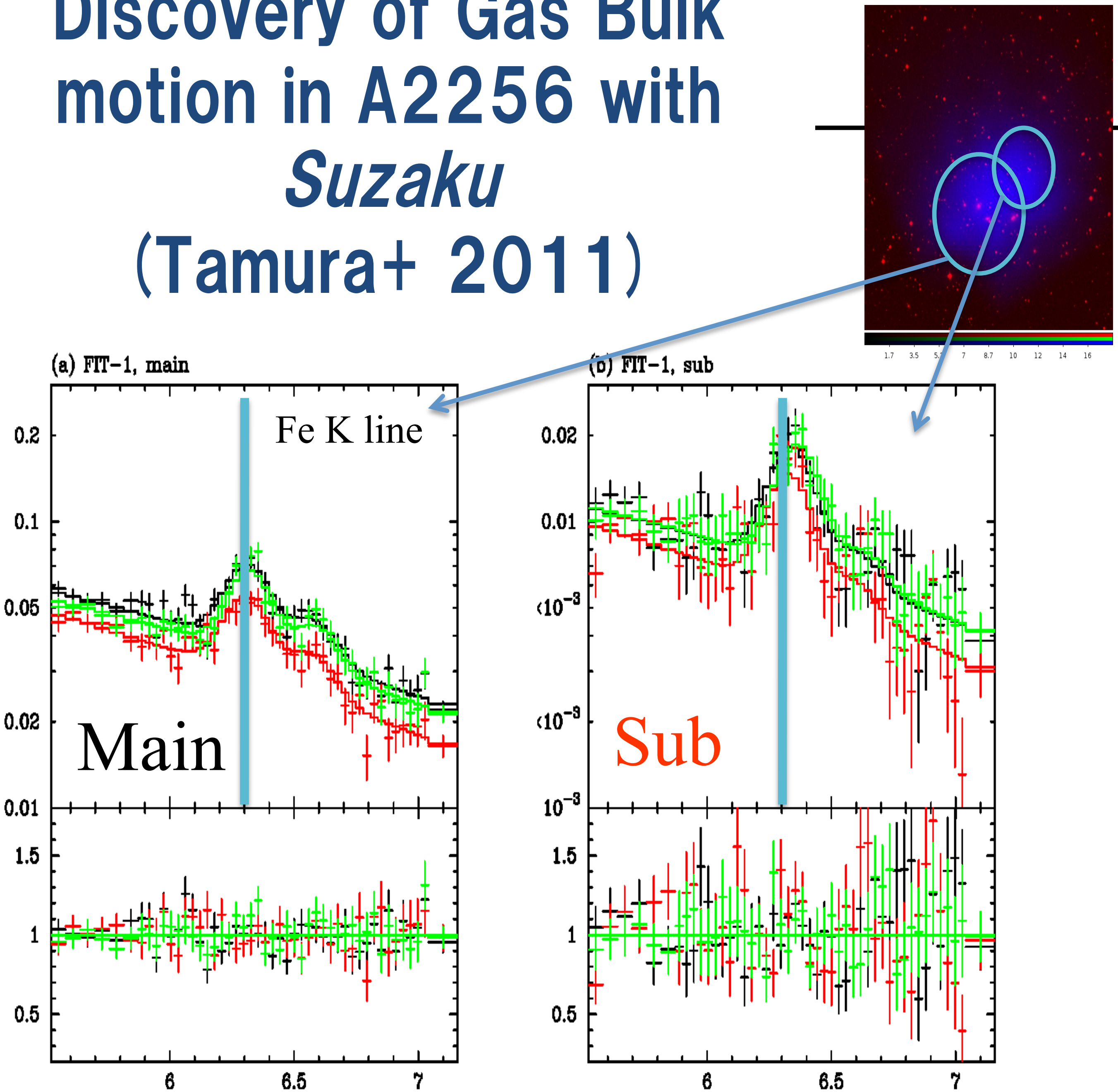

X-ray line center energies differs slightly but

Fe line profiles

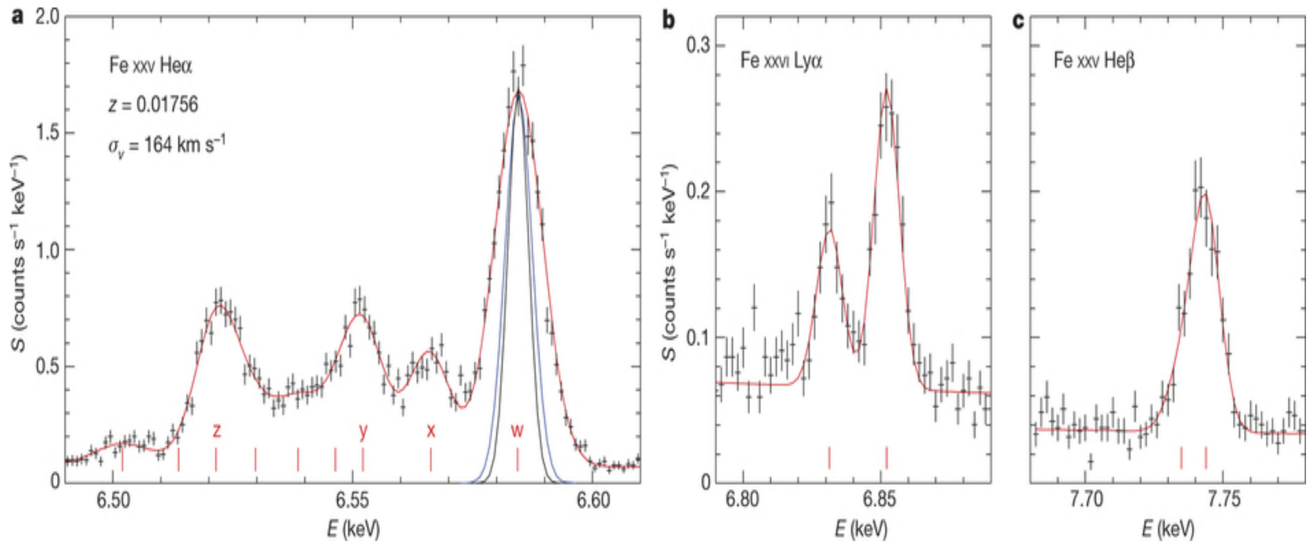

[H16; Fig.2] Spectra of Fe XXV Heα, Fe XXVI Lyα and Fe XXV Heβ from the outer region. Gaussians (red curves) were fitted to lines with energies (marked by short red lines) from laboratory measurements in the case of He-like Fe XXV (a, c) and from theory in the case of Fe XXVI Lyα (b; see Extended Data Table 1 for details) with the same velocity dispersion (σv = 164 km s^{-1}), except for the Fe XXV Heα resonant line, which was allowed to have its own width. Instrumental broadening with (blue line) and without (black line) thermal broadening are indicated in a. The redshift (z = 0.01756) is the cluster value to which the data were self-calibrated using the Fe XXV Heα lines. The strongest resonance ('w'), intercombination ('x', 'y')

Spectral fits with the CIE model

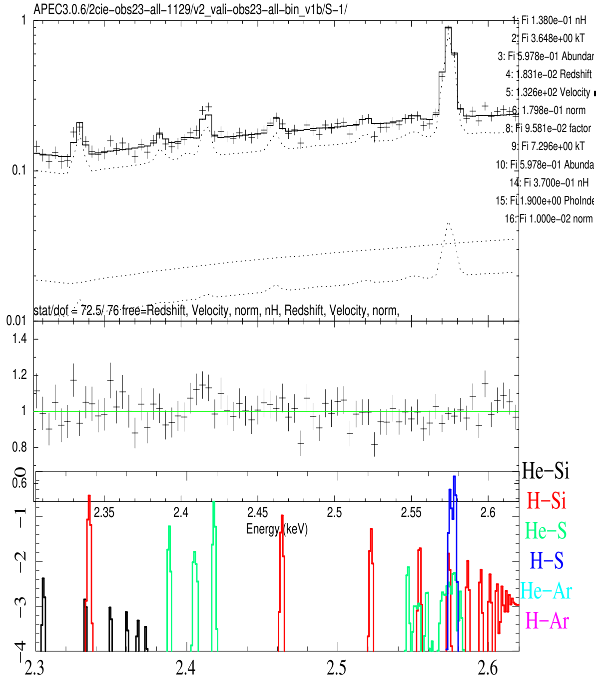

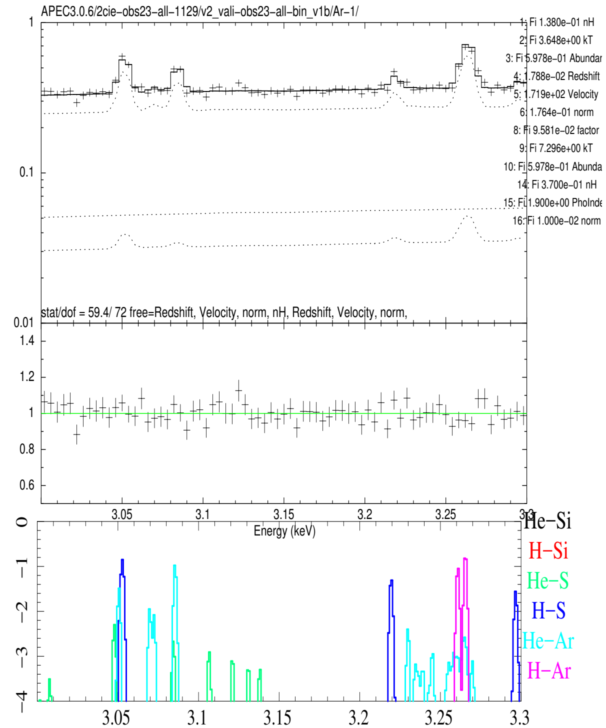

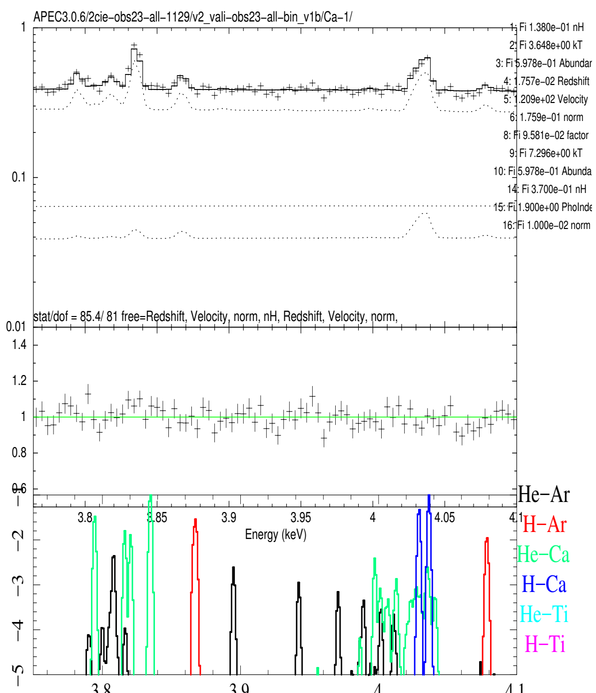

Line resolved spectrum ⇨ Robust measurement of thermal structure ⇨ Accurate measurements of elemental abundances, Si,S,Ar,Ca,Cr, Mn, Fe, and Ni

⇨ close to the solar ratio

⇨ Origin of metals and

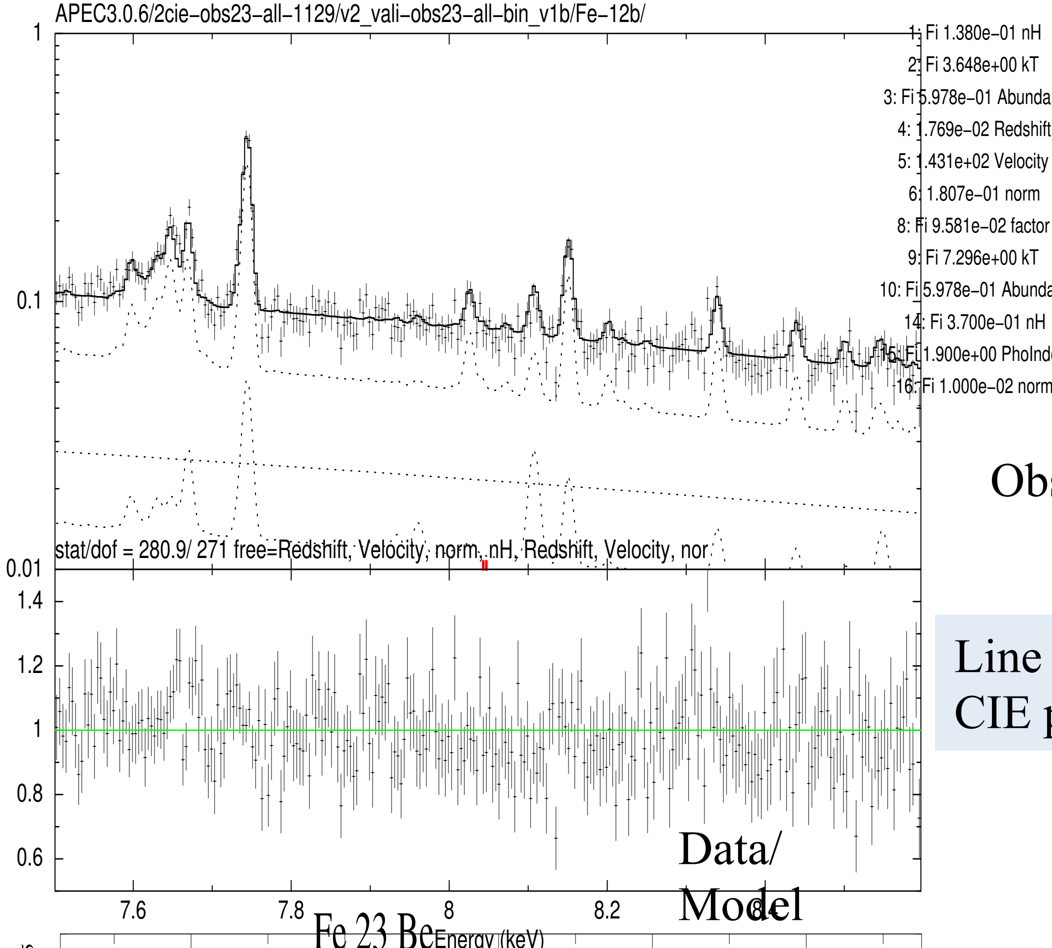

Same model as the previous page, but different normalization and redshift (to compensate calibration

Obs23 full-fov

Line flux ratios ⇨ CIE prediction

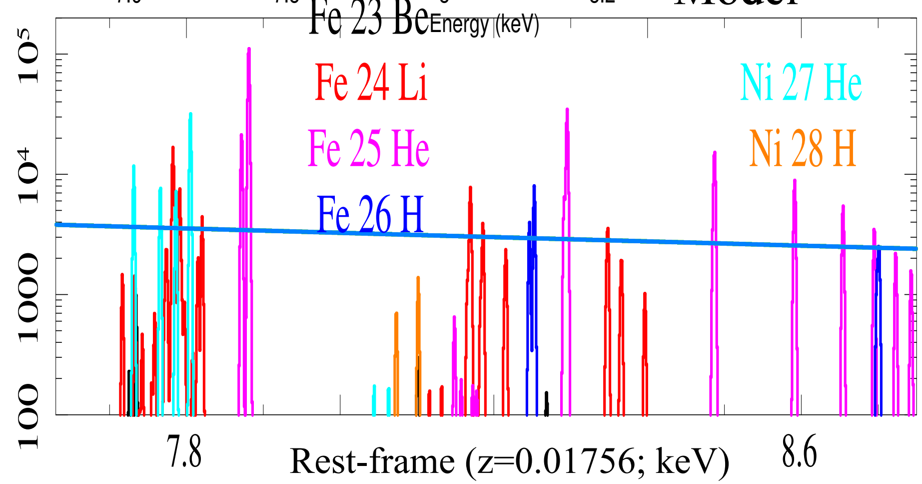

Line emission model (SPEX/CIE/ 4keV)

CIE fitting: Reduction of the Fe-resonance

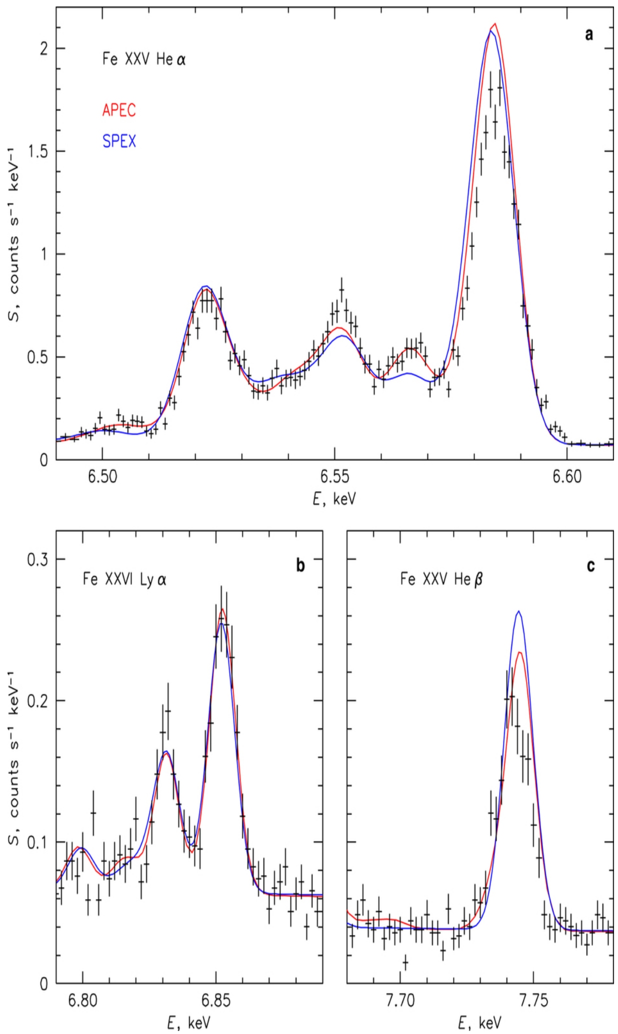

From Nature (2016): Extended fig.2: The Fe line complexes from the outer region compared with best-fit models.

- ❖ Strong resonant transition toward the core: absorbed and re-emitted, $\tau > 1$.

centre of the cluster up to a radius of 1 Mpc, $\tau = \int n_i \sigma_0 \, dr$, where n_i is the ion concentration and the cross-section for a given ion is

$$\sigma_0 = \frac{\sqrt{\pi} h r_e c f}{\Delta E_D}, \quad (3)$$

where

$$\Delta E_D = E_0 \left(\frac{2kT_e}{A m_p c^2} + \frac{V_{turb}^2}{c^2} \right)^{1/2} = E_0 \left[\frac{2kT_e}{A m_p c^2} (1 + 1.4 A M^2) \right]^{1/2}. \quad (4)$$

In the above equations E_0 is the energy of a given line, A is the atomic mass of the corresponding element, m_p is the proton mass, V_{turb} is the characteristic turbulent velocity, M is the corresponding Mach number, r_e is the classical electron radius and f is the oscillator strength of a given atomic transition. The wavelengths and

(Churazov+ 2004)

Sloshing in the Perseus core

A sloshing model

- most of the bulk motions are likely driven by the gas sloshing in the core of the Perseus cluster.
- The molecular gas can be advected by the sloshing hot gas, resulting in their similar LOS velocities.

wakes of buoyantly rising bubbles

- Part of the observed large-scale motions of vbulk ~ 100 km s−1 might be due to streaming motions around and in the wakes of buoyantly rising bubbles as well.
- to the north of the core, the trend in the LOS velocities of the ICM is consistent with the trend in the velocities of the molecular gas within the northern optical emission line filaments (Salomé et al. 2011).
- These trends are consistent with the model where the optical emission line nebulae and the molecular gas result from thermally unstable cooling of low-entropy gas uplifted by buoyantly rising bubbles (e.g., Hatch et al. 2006; McNamara et al. 2016).

Comparisons with simulations

- Lau et al. (2017)
- Bourne and Sijacki (2017)

Smaller scale gas motions

- AGN feedback
  - Driven from the center ~ small scale.
  - Rising bubbles
  - Sound wave (Fabian+ 2017)
  - d
- Structure formation
  - Frequent minor mergers.
  - Galaxy motions.
  - ICM hydrodynamic and magneto-thermal instabilities.ddd
- Sloshing motions/cold fronts (e.g. ZuHone+ 2013).
  - Several cold fronts are seen in the X-ray images (e.g. Churazov et al. 2003).
  - The observed dispersion will abruptly change across the cold fronts, mostly located outside the Hitomi FOV.

Two sources of gas velocities

- AGN feedback
  - Driven from the center ~ small scale.
  - Rising bubbles
  - Sound wave (Fabian+ 2017)
- ← Observed turbulent velocity

- Structure formation
  - Major merger and accretion flow→ Large (~Mpc) eddies → cascade/dissipate in smaller scale (Re~1)
  - Large scale motion → Non-Gaussian velocity.
  - Radially increased V_{turb} , due to incraese of effective projected length
  - Frequent minor mergers
  - Galaxy motions
  - Sloshing motions/cold fronts

Predictions: Detect and locate ICM turbulence

Perseus, 100ks, 3’×3‘ → 11,000 cts in He-like Fe

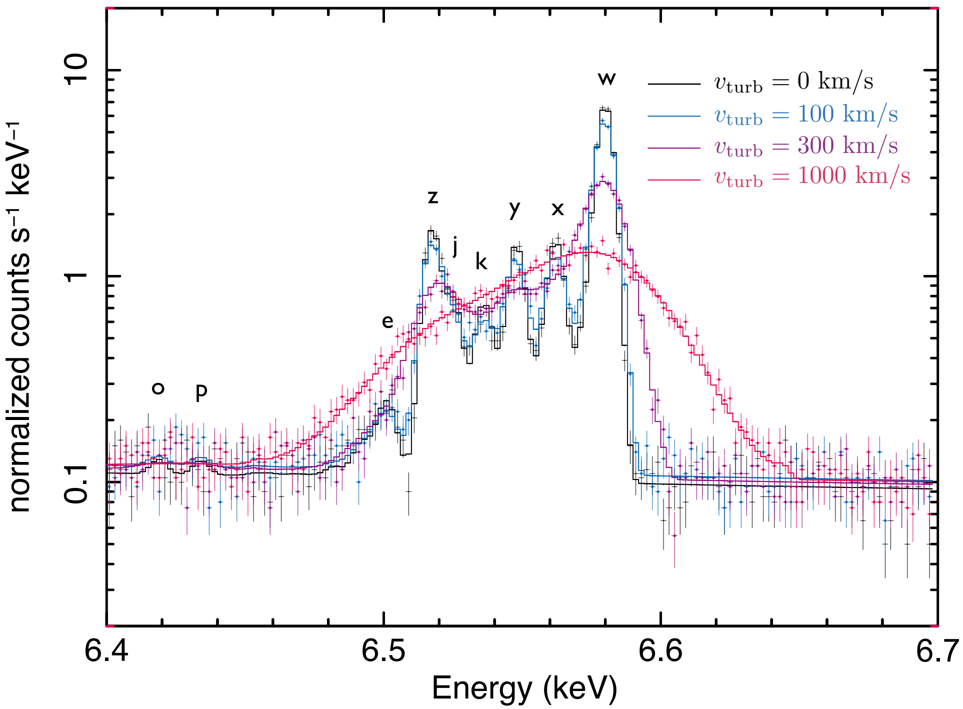

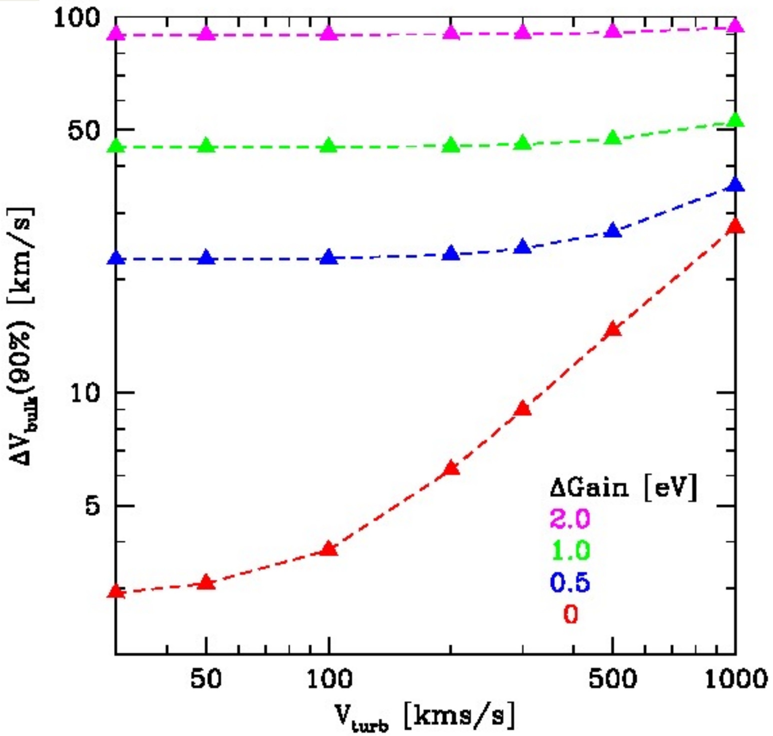

$$
\begin{aligned}
W_{\rm inst} &\simeq 5\ {\rm eV}, \\
W_{\rm therm} &= \sqrt{8\ln 2}\left(\frac{kT_{\rm ion}}{m_{\rm ion}c^2}\right)^{1/2} E_{\rm obs}, \\
&= 4.9\ {\rm eV}\left(\frac{kT_{\rm ion}}{5\ {\rm keV}}\right)^{1/2}\left(\frac{m_{\rm ion}}{56\ m_{\rm p}}\right)^{-1/2}\left(\frac{E_{\rm obs}}{6.7{\rm keV}}\right), \\
W_{\rm turb} &= \sqrt{8\ln 2}\left(\frac{v_{\rm turb}}{c}\right) E_{\rm obs}, \\
&= 5.3\ {\rm eV}\left(\frac{v_{\rm turb}}{100\ {\rm km/s}}\right)\left(\frac{E_{\rm obs}}{6.7\ {\rm keV}}\right),
\end{aligned}
$$

Gain errors (∼2.0 eV) dominate
if counts >100 & $V_{\rm turb}$ < 300 km/s

Outline

1. Motivations: X-ray spectroscopy and cluster dynamics and related physics
2. *Hitomi*, and 1st X-ray carorimeter. Observations of the Perseus cluster core.
3. Results (1) Line profile and the ICM velocities
4. Results (2) Spectral fitting with collisional ionization equilibrium models and thermal structure
5. Discussion
6. Summary

Interaction in a cluster (Energy flows)